Redox Biology 62 (2023) 102655

Contents lists available at ScienceDirect

Redox Biology

journal homepage: www.elsevier.com/locate/redox

miR-125b-5p in adipose derived stem cells exosome alleviates pulmonary microvascular endothelial cells ferroptosis via Keap1/Nrf2/GPX4 in sepsis lung injury

Kuo Shen [a,1], Xujie Wang [a,1], Yunwei Wang [a,1], Yanhui Jia [a,1], Yue Zhang [a], Kejia Wang [a], Liang Luo [a], Weixia Cai [a], Jin Li [a], Shaohui Li [a], Yuting Du [a], Lixia Zhang [a], Hao Zhang [a], Yuxi Chen [a], Chaolei Xu [a], Jinxin Zhang [b], Ruizhi Wang [a], Xuekang Yang [a,***], Yunchuan Wang [a,**], Dahai Hu [a,*]

[a] Department of Burns and Cutaneous Surgery, Xijing Hospital, Fourth Military Medical University, Chang-Le Xi Street #127, Xi'an, 710032, China
[b] Department of Emergency, Xijing Hospital, Fourth Military Medical University, Chang-Le Xi Street #127, Xi'an, 710032, China

ARTICLE INFO

Keywords:
ADSCs exosome
Sepsis
Acute lung injury
Ferroptosis
GPX4
Nrf2

ABSTRACT

Background: Sepsis is a fatal disease with a high rate of morbidity and mortality, during which acute lung injury is the earliest and most serious complication. Injury of pulmonary microvascular endothelial cells (PMVECs) induced by excessive inflammation plays an important role in sepsis acute lung injury. This study is meant to explore the protective effect and mechanism of ADSCs exosomes on excessive inflammation PMVECs injury.
Results: We successfully isolated ADSCs exosomes, the characteristic of which were confirmed. ADSCs exosomes reduced excessive inflammatory response induced ROS accumulation and cell injury in PMVECs. Besides, ADSCs exosomes inhibited excessive inflammatory response induced ferroptosis while upregulated expression of GPX4 in PMVECs. And further GPX4 inhibition experiments revealed that ADSCs exosomes alleviated inflammatory response induced ferroptosis via upregulating GPX4. Meanwhile, ADSCs exosomes could increase the expression and nucleus translocation of Nrf2, while decrease the expression of Keap1. miRNA analysis and further inhibition experiments verified that specific delivery of miR-125b-5p by ADSCs exosomes inhibited Keap1 and alleviated ferroptosis. In CLP induced sepsis model, ADSCs exosomes could relieve the lung tissue injury and reduced the death rate. Besides, ADSCs exosomes alleviated oxidative stress injury and ferroptosis of lung tissue, while remarkably increase expression of Nrf2 and GPX4.
Conclusion: Collectively, we illustrated a novel potentially therapeutic mechanism that miR-125b-5p in ADSCs exosomes could alleviate the inflammation induced PMVECs ferroptosis in sepsis induced acute lung injury via regulating Keap1/Nrf2/GPX4 expression, hence improve the acute lung injury in sepsis.

1. Background

Sepsis is a fatal disease, with a high rate of morbidity, particularly in intense care units. Sepsis brought huge burden on both patients and healthcare system throughout the world [1]. It is estimated that sepsis claimed as many as 1.7 million lives throughout the world [2]. Most noteworthy is that of all complications of sepsis, acute lung injury is the earliest and the most serious one [3]. Macrophages and pulmonary microvascular endothelial cells (PMVECs) are the most important mediators and victims of acute lung injury [4]. Upon foreign pathogen invading, alveolar macrophages (AMs), tissue-derived macrophages in lung tissue, were activated and polarized to a pro-inflammatory M1 phenotype, which secreted inflammatory cytokines such as tumor necrosis factor-α (TNF-α), interleukin 1 (IL-1), and interleukin 6 (IL-6) [5,6]. Excessive inflammatory cytokines and ROS attack cytomembrane and DNA of PMVECs, leading to injury of PMVECs [7]. Impaired

* Corresponding author.
** Corresponding author.
*** Corresponding author.
E-mail addresses: yangxuekangburns@163.com (X. Yang), wangyunchuan@fmmu.edu.cn (Y. Wang), hudahaidoc@163.com (D. Hu).
[1] Those authors contributed equally.

https://doi.org/10.1016/j.redox.2023.102655
Received 25 January 2023; Received in revised form 20 February 2023; Accepted 2 March 2023
Available online 9 March 2023

PMVECs lead to increase of vascular permeability, resulting in more infiltration of more inflammatory cell (neutrophils and bone marrow–derived monocytes), and thus lead to worsen damage [8]. There is no doubt that the more inflammatory cytokines produced, the better foreign pathogen eliminated. However, undue inflammatory cytokines storm and ROS production lead to tissue damage [9]. Hence, how to mitigate PMVECs injury and restore cell function and integrity of vessel is an important therapeutic target in treatment of sepsis induced acute lung injury.

Ferroptosis, a unique modality of cell death, is driven by iron-dependent phospholipid peroxidation, and regulated by multiple cellular metabolic pathways, including redox homeostasis, iron handling, mitochondrial activity and metabolism of amino acids, lipids and sugars, in addition to various signaling pathways relevant to disease [10,11]. It is reported that ferroptosis plays a crucial role in the initiation and progression of many diseases, such as seizure, acute liver injury and acute lung injury [12–16]. Studies reported that ferroptosis is involved in multiorgan dysfunction syndrome (MODS), which is common in sepsis patients [17]. The sequential organ failure assessment (SOFA) score of 176 critically ill adult patients were positively correlated with levels of malondialdehyde and catalytic iron, markers of lipid peroxidation, in plasma [17]. Studies indicated that excessive ferroptosis would aggravate the damage in the acute lung injury, while alleviating ferroptosis by various antioxidant would improve the tissue damage [18,19]. GPX4, an important antioxidant enzyme, is an important negative regulator of ferroptosis by reducing lipid peroxidation [20,21]. Inactivation or degradation of GPX4 induces accumulation of lipid peroxides, leading to ferroptosis, while upregulation of GPX4 effectively inhibits ferroptosis [21,22]. Besides, nuclear factor E2-related factor 2 (Nrf2), a master transcription factor, regulates a wide variety of cytoprotective genes including GPX4 [23]. Upregulation of Nrf2 would exert protective effect in lung injury via inducing expression of GPX4 and reducing ferroptosis [11].

As an important means of intercellular communication, ADSCs exosome is a promising mediator in tissue repair and regeneration after injury [24,25]. Studies have shown that exosomes from different sources have different regulatory effects on target cells. Exosomes from inflammatory or injury cells could exert harmful effect on receiving cells, while exosomes from stem cells can not only promote the repair and regeneration of damaged tissue but also suppress inflammation and exert protective effect in a range of inflammatory diseases, including sepsis, acute respiratory distress, etc [26–28]. There are multiple components contained in exosomes, such as nucleic acid, protein, and lipid, which account for the regulative effect of exosomes. MiRNA is the most important components in exosomes which transfers into receiving cells and regulates biological process of receiving cells. Emerging studies indicated that ADSCs exosomes can improve CLP induced organ damage through suppressing excessive inflammatory response [29,30]. Our previous study indicated that ADSCs exosomes can regulate Keap1/Nrf2 pathway in macrophage and lung tissue, thus exert protective effect in CLP induced lung injury [29]. However, whether ADSCs exosomes can protect PMVECs form ferroptosis via Keap1/Nrf2/GPX4 pathway is still unclear. Consequently, in this study, we investigated the anti-oxidative effect of ADSCs exosomes and relationship with Keap1/Nrf2/GPX4 axis. The results indicated that ADSCs exosomes can significantly alleviate inflammation response induced PMVECs ferroptosis. Besides, when pretreated with ADSCs exosomes, GPX4 expression was more pronounced. Inhibition of GPX4 by RSL3 revealed that when GPX4 was inhibited, anti-ferroptosis effect of ADSCs exosomes was diminished. What is more, miRNA analysis results indicated regulative effect of ADSCs exosome on Keap1/Nrf2/GPX4 axis depend on delivery of miR-125b-5p. And in CLP generated sepsis model, administration of ADSCs exosomes could reduce mortality of sepsis mice. Use of ADSCs exosomes ameliorated lung injury as well as ferroptosis while Nrf2 and GPX4 was potently upregulated. Collectively, this study revealed that ADSCs exosomes relieved inflammation induced PMVECs ferroptosis and protected lung injury from sepsis via Keap1/Nrf2/GPX4 axis.

2. Results

2.1. Characterization of ADSCs and exosomes

Primary ADSCs isolated from adipose tissue showed a spindle-shape in inverted microscope (Fig. 1A). As shown in Fig. 1B, specific mesenchymal stem cell surface markers CD29, CD44, CD73 and CD90 were positively expressed in primary ADSCs, while CD34 and CD45 almost not expressed. These results confirmed the characterization of ADSCs. Then, we extracted the exosomes and authenticated it with TEM, western blot and NTA. The isolated vesicles presented a cup-shape typical exosome morphology with double-layer membrane structure under TEM (Fig. 1C). Western blot showed that widely recognized molecular markers for exosomes CD63, CD9 and TSG101 were highly expressed in isolated particles (Fig. 1D), while β-Actin was negatively expressed. Moreover, NTA results showed that the particle diameters ranged from 50 to 150 nm, with an average of 117.5 nm (Fig. 1E). Besides, CD31 immunofluorescence results indicated that isolated cells from pulmonary capillaries were positively stained with CD31, indicating that we successfully isolated PMVECs (Fig. 1F). As shown in Fig. 1G, PKH26 labeled exosomes could be absorbed by PMVECs. These results in all indicated that we successfully isolated ADSCs exosomes and PMVECs.

2.2. ADSCs exosomes improved inflammatory response induced PMVECs injury

Primary PMVECs were successfully isolated from newly-born mice lung tissue. 1 μg/mL LPS were added to RAW264.7 cells to activated macrophage. ELISA results indicated that IL-1β and TNF-α content in LPS treated RAW264.7 cells were significantly increased (Fig. S1A). And PCR results confirmed surge of inflammatory cytokines (IL-1β, TNF-α and IL-6) in LPS treated RAW264.7 cells (Fig. S1B). Conditioned medium (CM) of LPS induced RAW264.7 cells were added into PMVECs cells to induce injury. Meanwhile, ADSCs exosomes were added into PMVECs to protect from macrophage CM induced injury (Fig. 2A). CCK8 results indicated that cell viability of PMVECs were attenuated when treated with LPS induced macrophage CM (Fig. 2B). Besides, flow cytometry results indicated that apoptosis rate of PMVECs treated with LPS induced macrophage CM was significantly higher than without (Fig. 2C). However, when PMVECs were treated with ADSCs exosomes, the viability of PMVECs were rejuvenated (Fig. 2B), and the apoptosis rate was decreased (Fig. 2D). Caspase3 immunofluorescence results also verified the up-regulative effect of macrophage CM on PMVECs apoptosis and the down-regulative effect of ADSCs. As is shown in Fig. 2D, fluorescence intensity of Ki67 was decreased when PMVECs were treated with LPS induced macrophage CM, but increased when ADSCs exosomes were used. And for tube formation assay, number of tube formation in macrophage CM group was lower than in control group as well as in ADSCs exosomes group (Fig. 2D). Furthermore, both *trans*-well and scratch assay revealed that macrophage CM impaired migration capability of PMVECs, while ADSCs exosomes could restore the migration capability. Hence, above results reveal that treatment with LPS induced macrophage CM damaged viability, proliferation, and migration of PMVECs, while ADSCs improved macrophage CM induced injury and decreased apoptosis.

2.3. ADSCs exosomes reduced inflammatory response induced ROS accumulation in PMVECs

To reveal the protective effect of ADSCs exosomes on macrophage CM stimulated PMVECs, ROS accumulation, DNA damage and antioxidant activity of differently treated PMVECs were detected. DCFH-DA was used to evaluate the ROS level in PMVECs. Flow cytometry and

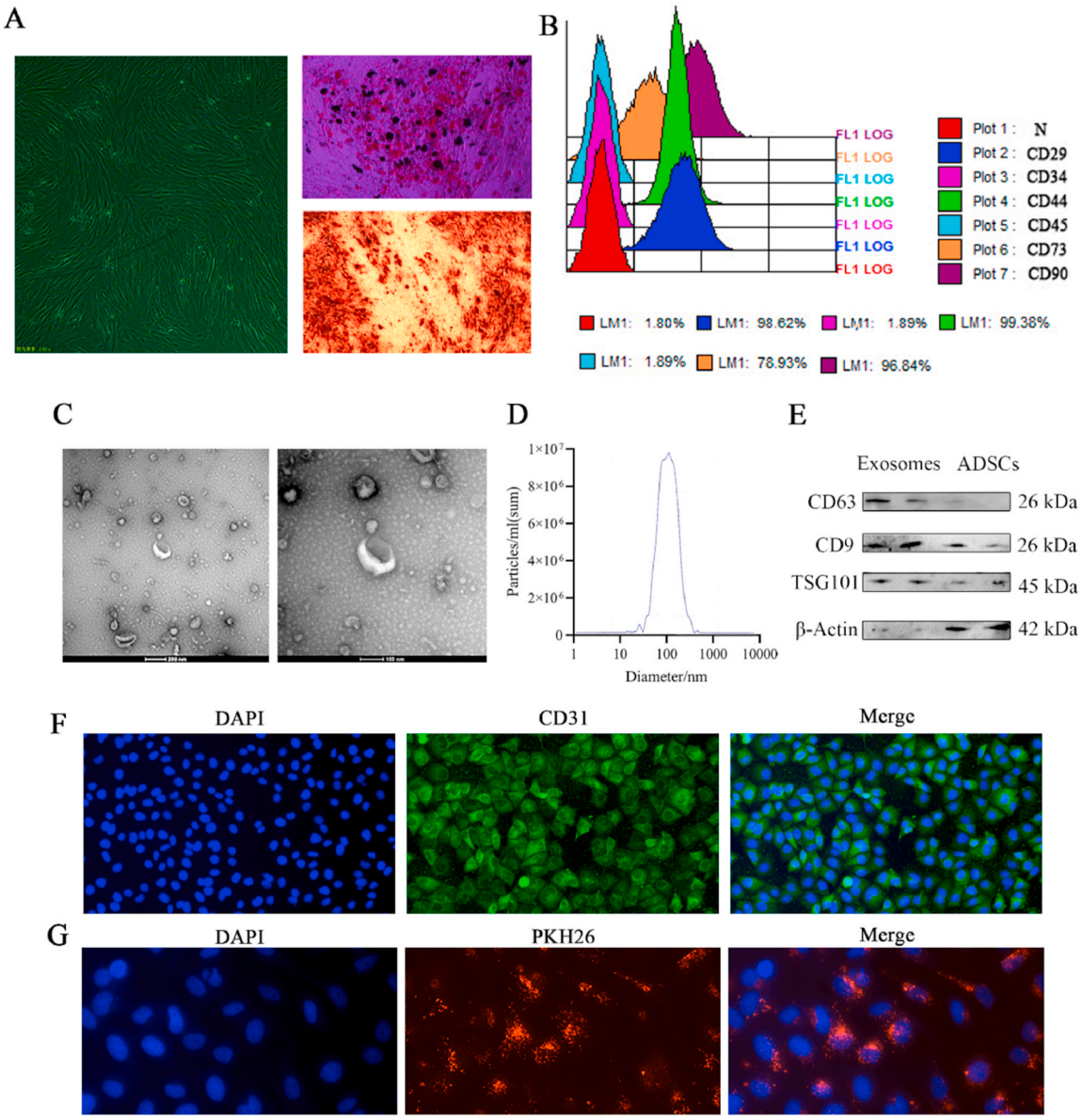

Fig. 1. Characterization of ADSCs and exosomes. A. Morphology of ADSCs observed by inverted microscope. Scale bar: 25 μm. B. Flow cytometry show ADSCs were positive for CD29 (98.62%), CD44 (99.38%), CD73 (78.39%), and CD90 (96.84%), negative for CD34 (1.89%) and CD45 (1.89%) negative. C. Morphology of ADSCs Exosomes detected by TEM. Scale bar: 200 nm (right); 100 nm (left). D. Diameters distribution of ADSCs exosomes detected by NTA (nm). E. β-Actin, TSG-101, CD63 and CD9 expressions of ADSCs exosomes were detected by western blot. F. CD31 immunofluorescent staining results of primary PMVECs, Blue: DAPI; Red: CD31, Magnification: 40x.G. ADSCs exosomes taken in by PMVECs. Red: PKH26 labeled ADSCs exosomes; Blue: DAPI. Magnification: 60x. (For interpretation of the references to colour in this figure legend, the reader is referred to the Web version of this article.)

immunofluorescence results indicated that ROS accumulation elevated significantly when PMVECs exposed to LPS induced macrophage CM (Fig. 3A&B), while ADSCs exosomes moderated the accumulation of ROS (Fig. 3A&B). As an indicator of DNA damage, 8-OHdG immunofluorescence results revealed that LPS induced macrophage CM could increase expression of 8-OHdG expression in PMVECs, while ADSCs exosomes counteracted the up-regulative effect of macrophage CM. Antioxidant enzymes activity plays an important role in balance of oxidative stress. Content of SOD and activity of CAT in PMVECs were decreased when exposed to LPS induced macrophage CM (Fig. 3D). As is shown in Fig. 3D, ADSCs exosomes could increase the content of SOD and activity of CAT in PMVECs. Mitochondrial membrane potential (MMP) is a key measure of mitochondrial functional status and an indicator of cell apoptosis, which could be measured by JC-1, a membrane potential sensitive dye. As Fig. 3E showed that most mitochondrial showed red fluorescence in control and ADSCs exosomes group, while green was predominant in fluorescence in LPS induced macrophage CM. that is, MMP in control and ADSCs exosomes group were higher than that of CM group. In short, exposing to LPS induced macrophage CM resulted in ROS accumulation and oxidative injury in PMVECs, but ADSCs exosomes reduced inflammatory response induced ROS accumulation and injury in PMVECs.

2.4. ADSCs exosomes reduced inflammatory response induced ferroptosis in PMVECs

Above results indicated that ADSCs exosomes could alleviate cell injury and ROS accumulation resulted from LPS induced macrophage CM in PMVECs. To verify the mechanism of regulative effect of ADSCs exosomes on inflammatory response induced injury in PMVECs, we

Fig.2

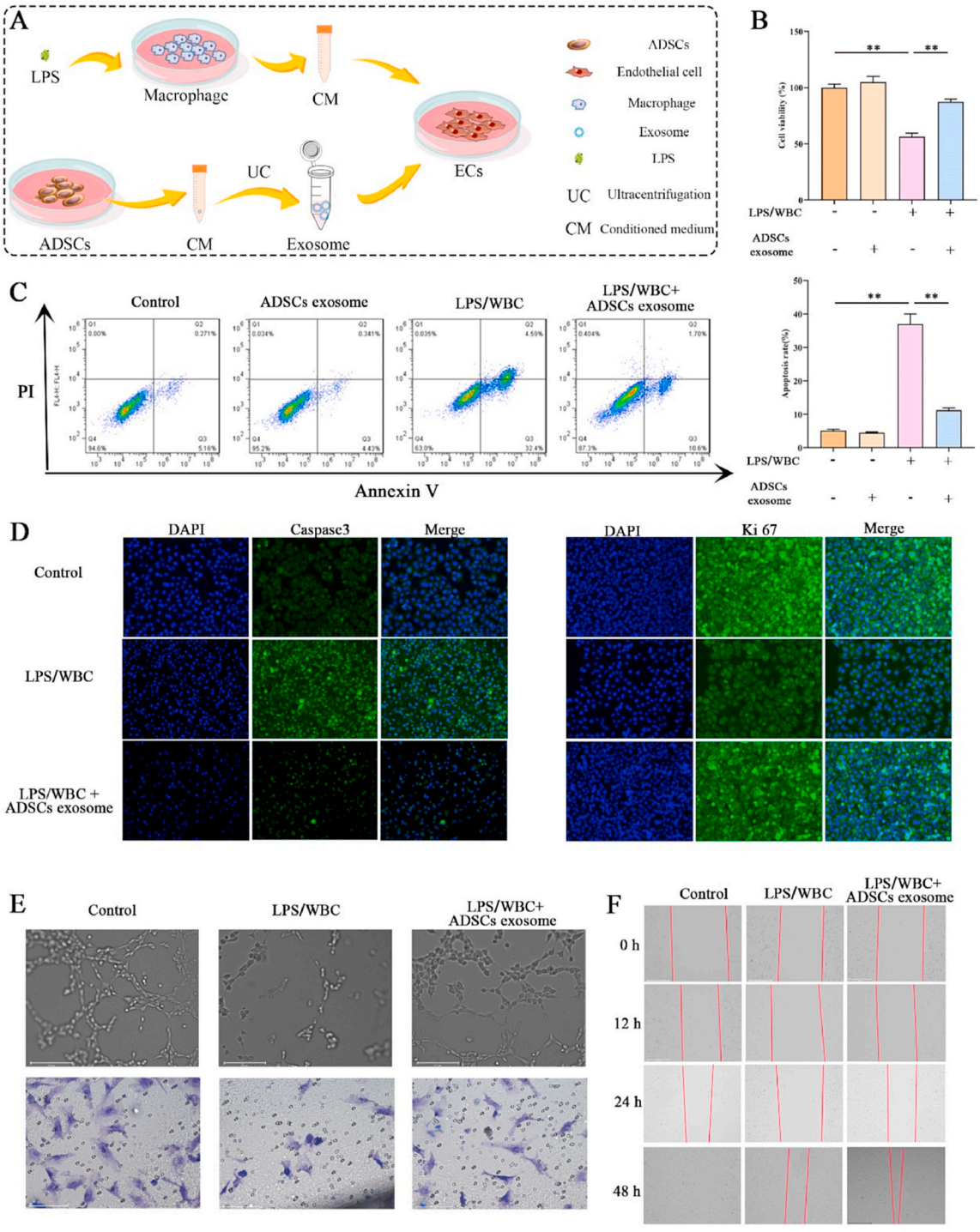

Fig. 2. ADSCs exosomes improved inflammatory response induced PMVECs injury. A. Schematic illustration of cell experiments. B. Cell viability of PMVECs after different treatments detected by CCK8, LPS/macrophage: LPS stimulated macrophage conditioned medium. * *: P ≤ 0.01. C. PI and Annexin V flow cytometry show apoptosis of PMVECs after different treatments, LPS/macrophage: LPS stimulated macrophage conditioned medium. * *: P ≤ 0.01. D. Caspase3 and Ki67 immunofluorescent staining results of differently treated PMVECs, Blue: DAPI; Green: Caspase3(left), Ki67(right), LPS/macrophage: LPS stimulated macrophage conditioned medium. * *: P ≤ 0.01. E. Angiogenesis and migration of differently treated PMVECs detected by cell tubule formation and *trans*-well assay respectively, LPS/macrophage: LPS stimulated macrophage conditioned medium (scale = 250 μm). F. Scratch wound assays show migration of PMVECs after different treatments, LPS/macrophage: LPS stimulated macrophage conditioned medium (scale = 250 μm). (For interpretation of the references to colour in this figure legend, the reader is referred to the Web version of this article.)

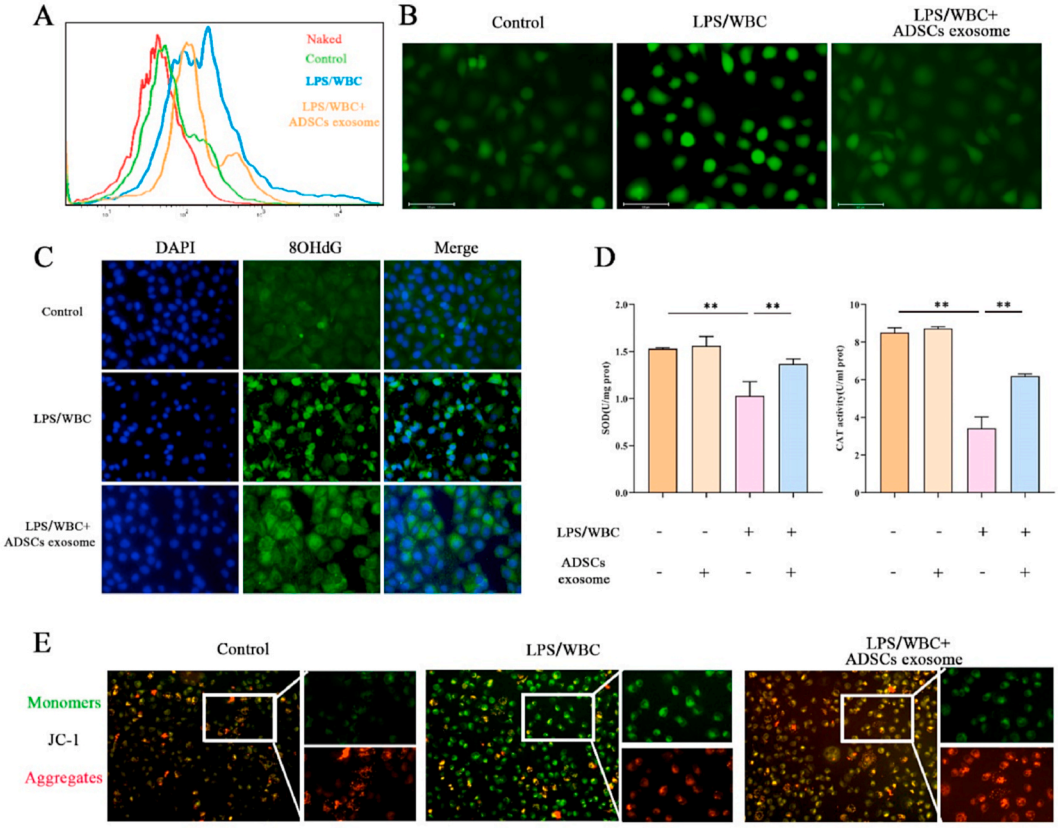

Fig. 3. ADSCs exosomes reduced inflammatory response induced ROS accumulation in PMVECs. A. ROS content of differently treated PMVECs detected by flow cytometry. B. ROS detected by immunofluorescence in differently treated PMVECs. Green: ROS. Magnification: 60x. C. 8OHdG immunofluorescent staining results of differently treated PMVECs, Blue: DAPI; Green: 8OHdg, LPS/macrophage: LPS stimulated macrophage conditioned medium. D. SOD and CAT content in differently treated PMVECs, LPS/macrophage: LPS stimulated macrophage conditioned medium, * *: P $\leq$ 0.01. E. JC1 staining show mitochondrial membrane potential of differently treated PMVECs, green fluorescence of the monomeric form of JC-1 in the cytosol after mitochondrial membrane depolarization (upper of each group), red fluorescence of the potential-dependent aggregation in the mitochondria (lower of each group), LPS/macrophage: LPS stimulated macrophage conditioned medium, * *: P $\leq$ 0.01. (For interpretation of the references to colour in this figure legend, the reader is referred to the Web version of this article.)

further detected ferroptosis related indicators. Level of lipid peroxidation were detected via 4-hydroxynonenal (4HNE) modifications and malondialdehyde (MDA). As is shown in Fig. 4A&B, LPS induced macrophage CM significantly increased lipid peroxidation expression of PMVECs, while ADSCs exosomes decreased the expression. Similarly, LPS induced macrophage CM and ADSCs exosomes exert same effects on other ferroptosis related indicators. Specifically, LPS induced macrophage CM downregulated expression of GSH and FRAP while increased expression of MDA. But ADSCs exosomes could mitigate CM induced GSH and FRAP downregulation and MDA increase (Fig. 4C). Further immunofluorescence results displayed that LPS induced macrophage CM increased fluorescence intensity of 4HNE and weaken fluorescence intensity of GPX4 (Fig. 4D). Not surprisingly, ADSCs exosomes could reverse changes triggered by LPS induced macrophage CM (Fig. 4D). In accord with immunofluorescence results, western blot results affirmed same regulative effect of LPS induced macrophage CM and ADSCs exosomes on 4HNE and GPX4 expression (Fig. 4E). Furthermore, western blot results showed slight increase of HO-1 and Nrf2 expression in CM treated PMVECs, while showed significant increase in ADCSs exosomes group (Fig. 4E). Above results in total indicated that LPS induced macrophage CM could increase ROS accumulation and ferroptosis level in PMVECs, while ADSCs exosomes could restore them.

2.5. ADSCs exosomes alleviated inflammatory response induced ferroptosis via upregulating GPX4 in PMVECs

GPX4, an important antioxidant enzyme, is a negative regulator of ferroptosis by reducing lipid peroxidation [20]. Inactivation or degradation of GPX4 induces accumulation of lipid peroxides, leading to ferroptosis, while upregulation of GPX4 effectively inhibits ferroptosis [31]. Above results indicated that ADSCs exosomes could inhibit ferroptosis as well as increasing GPX4. Whether ADSCs exosomes exert inhibition effect on ferroptosis in PMVECs via regulating GPX4 was further verified through GPX4 inhibition experiments. As is shown in Fig. 5A, when expression of GPX4 was inhibited by RSL3, cell viability and FRAP content in PMVECs decreased sharply even been treated with ADSCs exosomes. On the contrary, level of lipid peroxidation and its product increased significantly when expression of GPX4 was inhibited by RSL3. Besides, western blot results indicated that when PMVECs were treated with RSL3, expression of 4HNE and HO-1 increased significantly while GPX4 was significantly inhibited. When expression of GPX4 was inhibited by RSL3, protective effect of ADSCs exosomes on inflammatory response induced ferroptosis was abrogated. Namely, ADSCs exosomes alleviated inflammatory response induced ferroptosis via upregulating GPX4 in PMVECs.

2.6. ADSCs exosomes regulated expression of Nrf2 pathway in PMVECs

Nrf2 and Keap1 signaling pathway is one of the most crucial and classical cell defense and survival pathway that reduce oxidative stress via regulating downstream gene HO-1, GXP4 and NQO1, etc [32,33]. Thus, we detected expression of important component in Nrf2 pathway. As shown in Fig. 4E, western blot results indicated that expression of Nrf2 were slightly increased when exposed to LPS induced macrophage

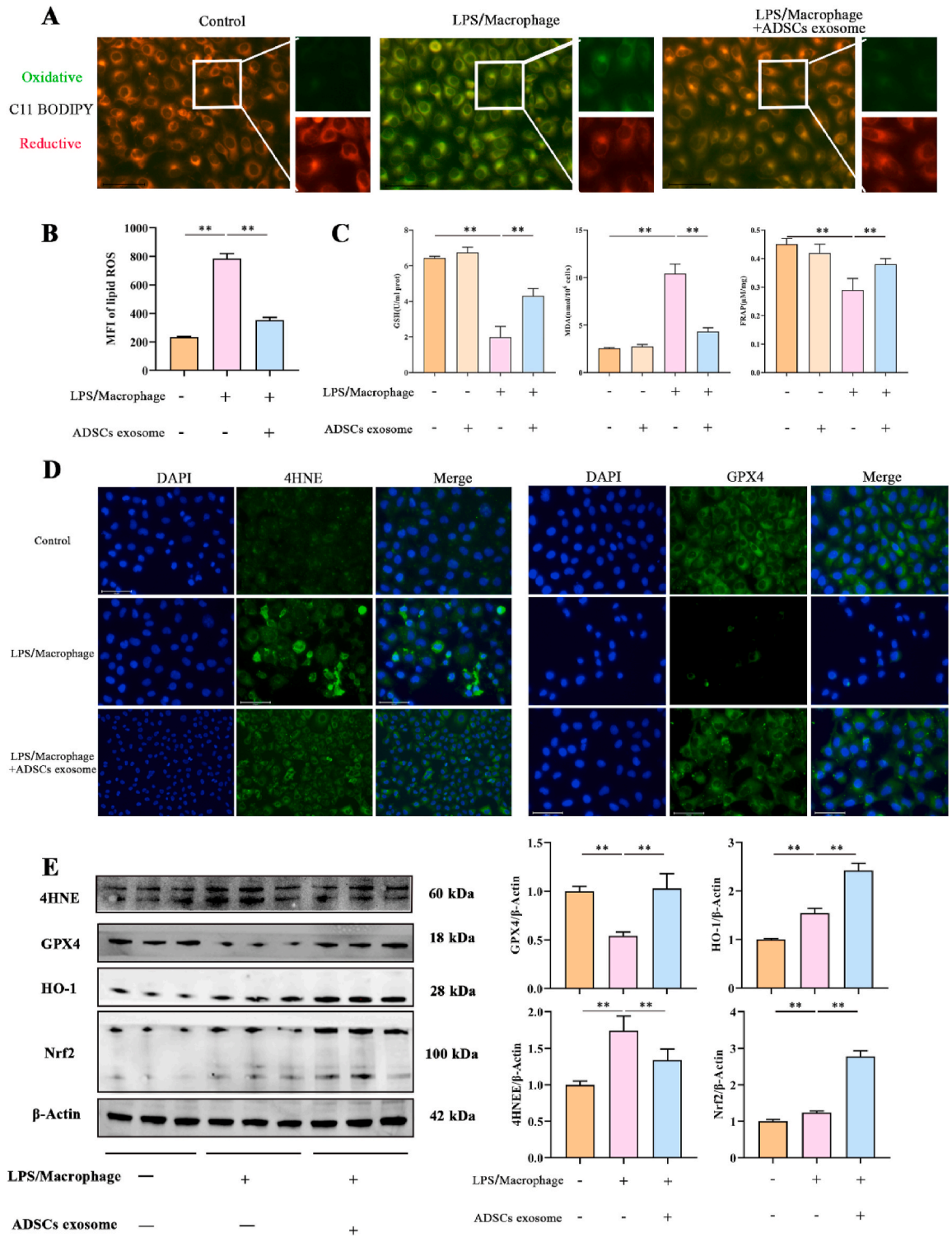

Fig. 4. ADSCs exosomes reduced inflammatory response induced ferroptosis in PMVECs. A. C11 BODIPY staining show lipid peroxidation of differently treated PMVECs, green fluorescence of the oxidative plasmolemma lipid (upper of each group), red fluorescence of the reductive plasmolemma lipid (lower of each group). B. Mean fluorescence intensity of lipid ROS of differently treated PMVECs, * *: P ≤ 0.01. C.GSH, MDA, and FRAP content in differently treated PMVECs, LPS/macrophage: LPS stimulated macrophage conditioned medium, * *: P ≤ 0.01. D. 4HNE (left) and GPX4(right) immunofluorescent staining results of differently treated PMVECs, Blue: DAPI; Green: 4HNE (left), GPX4 (right), LPS/macrophage: LPS stimulated macrophage conditioned medium. E.4HNE, GPX4, HO-1 and Nrf2 expressions of differently treated PMVECs were detected by western blot, LPS/macrophage: LPS stimulated macrophage conditioned medium, * *: P ≤ 0.01. (For interpretation of the references to colour in this figure legend, the reader is referred to the Web version of this article.)

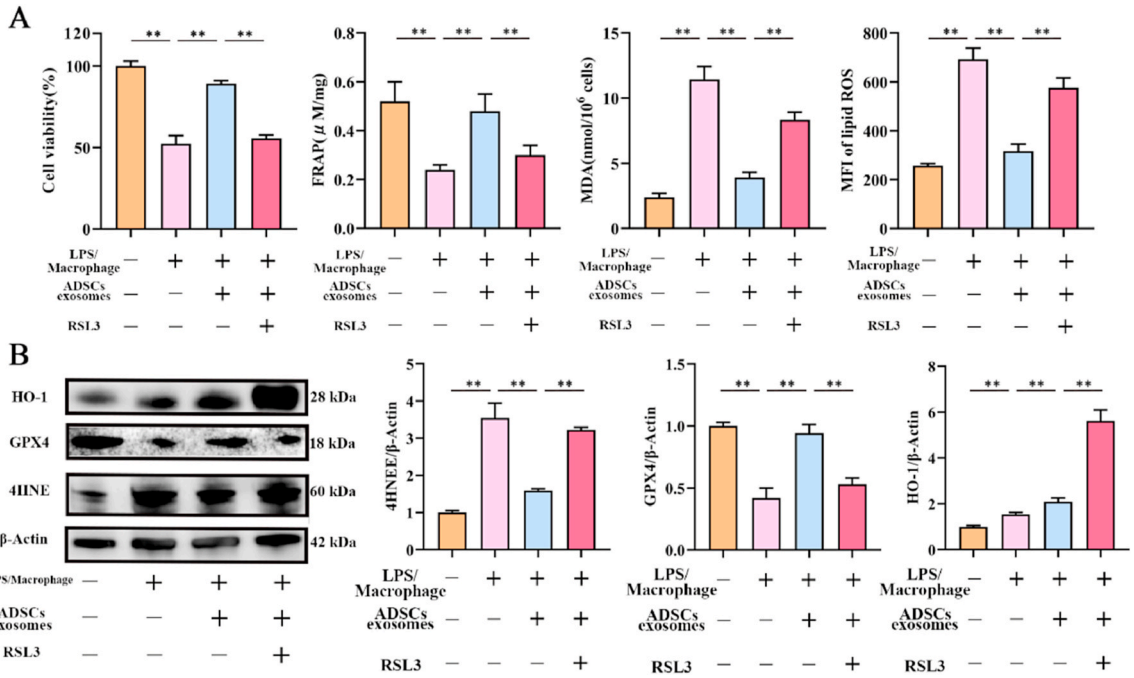

Fig. 5. ADSCs exosomes alleviated inflammatory response induced ferroptosis via upregulating GPX4 in PMVECs. A. Cell viability, FRAP, MDA and MFI of lipid ROS in PMVECs treated with LPS/macrophage, LPS/macrophage + ADSCs exosomes, and LPS/macrophage + ADSCs exosomes + RSL3, LPS/macrophage: LPS stimulated macrophage conditioned medium. * *: $P \leq 0.01$. B. 4HNE, GPX4 and HO-1 expressions PMVECs treated with LPS/macrophage, LPS/macrophage + ADSCs exosomes, and LPS/macrophage + ADSCs exosomes + RSL3were detected by western blot, LPS/macrophage: LPS stimulated macrophage conditioned medium, * *: $P \leq 0.01$.

CM, but significantly boosted when treated with ADSCs exosomes. Besides, ADSCs exosomes could increase expression of downstream antioxidative gene HO-1 and GXP4 (Fig. 4E). And western blot and PCR results also indicated that ADSCs exosomes could increase expression of Nrf2, while downregulated expression of Keap1, the negative regulator of Nrf2 (Fig. 6A&B). Nrf2 proteins in cytoplasm and nucleus were detected by western blot, and results indicated that ADSCs exosomes could increase cytoplasm Nrf2 expression slightly, while increase nucleus Nrf2 expression greatly (Fig. 6C). To sum up, above in vitro experiments revealed that ADSCs exosomes could alleviate LPS induced macrophage CM induced ROS accumulation, oxidative injury and ferroptosis via regulating Keap1/Nrf2/GPX4 axis.

2.7. *ADSCs exosomes regulated Nrf2 pathway in PMVECs via delivery of miR-125b-5p*

It is universally acknowledged miRNA, as well as other components, is one of the most important cargos that exosomes transport into recipient cell. To draw miRNA expression profile of ADSCs exosomes, a microarray analysis was conducted. As shown in Fig. 7A, as many as 63

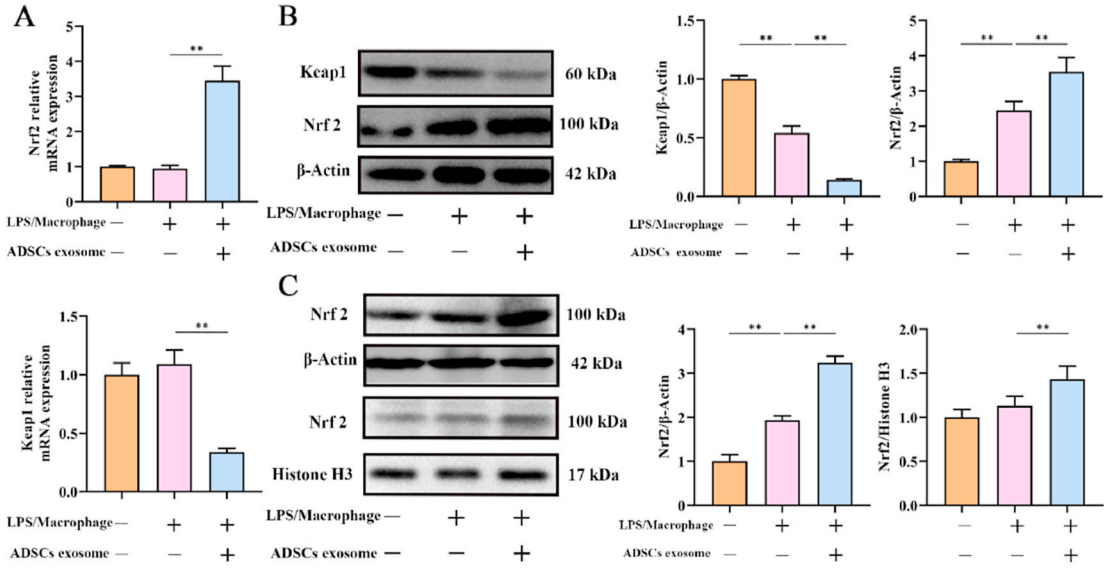

Fig. 6. ADSCs exosomes regulated expression of Nrf2 pathway in PMVECs. A. Nrf2 and Keap1 mRNA expressions in different PMVECs cells detected by PCR. **: $P \leq 0.05$ B Nrf2 and Keap1 protein expressions in different PMVECs cells detected by western blot. C. Nrf2 expressions in the cytoplasm and nuclei of different PMVECs detected by western blot. LPS/macrophage: LPS stimulated macrophage conditioned medium, * *: $P \leq 0.01$.

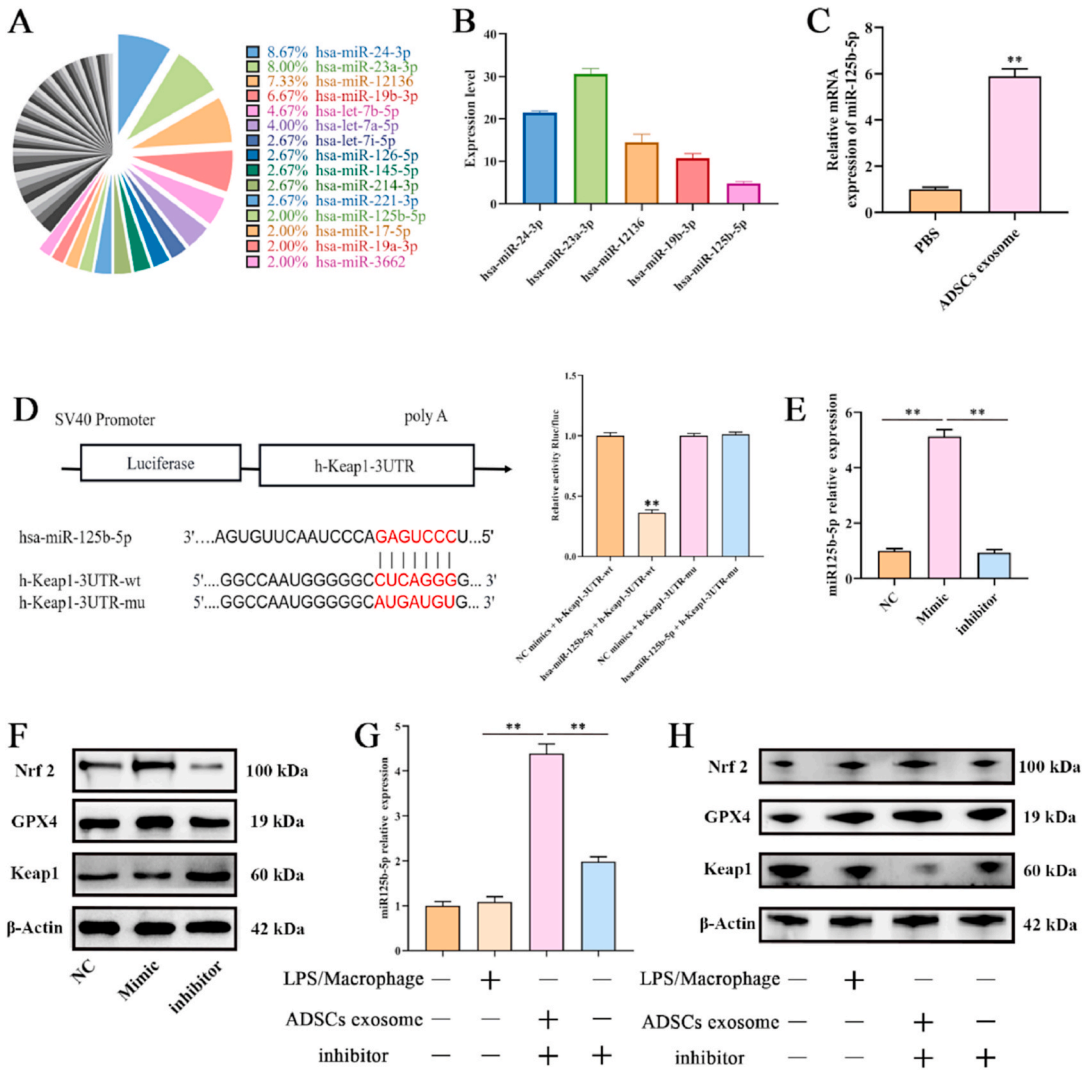

Fig. 7. ADSCs exosomes regulated Nrf2 pathway in PMVECs via delivery of miR-125b-5p A. miRNA microarray results indicating relative percentage of miRNAs in total miRNA reads. B. PCR results of 5 miRNAs (miR-24-3p, miR-23a-3p, miR-12136, miR-19b-3p, and miR-125b-5p) expression in ADSCs exosomes. C. PCR results indicating miR-125b-5p expression in PBS and ADSCs exosomes treated PMVECs. D. Structure and luciferase result of dual luciferase reporter gene. E. PCR results indicating miR-125b-5p expression in NC, miR-125b-5p expression mimic and inhibitor treated PMVECs. F. Western blot results of Keap1, Nrf2, and GPX4 expression in NC, miR-125b-5p expression mimic and inhibitor treated PMVECs. G. PCR results indicating miR-125b-5p expression in differently treated PMVECs. H. Western blot results indicating Keap1, Nrf2, and GPX4 expression in differently treated PMVECs. LPS/macrophage: LPS stimulated macrophage conditioned medium, * *: $P \leq 0.01$.

identified miRNAs were detected in ADSCs exosomes. The top 15 most abundant miRNAs were miR-24-3p, miR-23a-3p, miR-12136, miR-19b-3p, let-7b-5p, let-7a-5p, let-7i-5p, miR-126-5p, miR-145-5p, miR-214-3p, miR-221-3p, miR-125b-5p, miR-17-5p, miR-19a-3p, miR-3662, and miR-423-5p, which make up more than half quantity of all the miRNAs. To predict the potential target genes of detected miRNAs, the miRDB, miRtarbase, starBase and TargetScan database were explored and predict target genes were further studied. What is noteworthy is that Keap1 is a predict the potential target of miR-125b-5p, which is enriched in ADSCs exosomes. Then, qRT-PCR results confirmed that miR-125b-5p as well as other enriched miRNA was expressed in ADSCs exosomes (Fig. 7B). Besides, when PMVECs were treated with ADSCs exosomes, expression of miR-125b-5p increased greatly (Fig. 7C). Subsequently, dual luciferase reporter analysis was conducted to verify the regulative effect of miR-125b-5p on Keap1. As is shown in Fig. 7D, overexpression of miR-125b-5p impaired activity of the Keap1-3′UTR-wt reporter, but there was no notable activity shift within mutated reporter. Namely, Keap1 is a regulative target of miR-125b-5p and miR-125b-5p can bind to 3′UTR of Keap1 gene. To further verify the regulative effect of miR-125b-5p on Keap1, we designed and synthesized the mimic and inhibitor of miR-125b-5p, and transfected them into PMVECs. As is shown in Fig. 7E, expression of miR-125b-5p was significantly promoted by mimic, while stay unchanged by inhibitor. Besides, when expression of miR-125b-5p was increased by mimic, expression of Keap1 was suppressed, while expression of Nrf2 and GPX4 was increased. Likewise, inhibitor increased expression of Keap1, while decreased expression of Nrf2 and GPX4(Fig. 7F). Moreover, we transfected ADSCs exosomes with inhibitor, added it into PMVECs and compared its regulative effect on Keap1 pathway with ADSCs exosomes. Results indicated that when expression of miR-125b-5p in ADSCs exosomes was inhibited by inhibitor (Fig. 7G), downregulation of Keap1 and upregulation of Nrf2 and GPX4 were mitigated (Fig. 7H). That is, when expression of miR-125b-5p in ADSCs exosome was inhibited, regulative effect of ADSCs exosome on Keap1/Nrf2/GPX4 axis were counteracted. Collectively, regulative effect of ADSCs exosome on Keap1/Nrf2/GPX4 axis depend on delivery of miR-125b-5p.

2.8. ADSCs exosomes alleviated CLP induced acute lung injury in mice

To detect the protective effect of ADSCs exosomes on acute lung injury of sepsis, as is shown in Fig. 8A, we established CLP sepsis models and treated with ADSCs exosomes. Results indicated that half of the mice in CLP group were dead at 24 h, and 80% at 48 h (Fig. 8B). While treated with ADSCs exosomes, the mortality declined to 10% at 24 h, and 60% at 48 h (Fig. 8B). Lung tissues were collected for HE staining and injury scoring via lung injury score, bronchoalveolar lavage fluid (BALF) and wet/dry ratio analyses. Protein concentration in BALF and the wet/dry ratio of mice in the CLP group were significantly higher than that of sham group as well as ADSCs exosomes group (Fig. 8C). HE results indicated that compared with the sham group, alveolar capillaries were swollen and congested, and the alveolar cavity was bleeding, accompanied by the infiltration of inflammatory cells in CLP group (Fig. 8D). Whereas ADSCs exosomes significantly improved above injury. Besides, CLP increased scores of mice lung injury score while ADSCs exosomes brought it down (Fig. 8E). Consequently, ADSCs exosomes alleviated CLP induced acute lung injury in mice.

2.9. ADSCs exosomes alleviated CLP induced inflammatory response in mice

The inflammatory response in mice after CLP and ADSCs exosomes treatment was detected by inflammatory cytokines detection by ELISA and PCR, MPO immunohistochemical staining, and macrophage markers immunofluorescence staining in lung tissues and serum. As Fig. S2A showed that both serum and BALF contents of TNF-α and IL-1β were significantly increased when treated with CLP, while the contents were downregulated by ADSCs exosomes. What is more, iNOS and Arg-1 double immunofluorescence staining results indicated that number of iNOS positive cells and iNOS fluorescence intensity in CLP group was well over that of sham and ADSCs exosome group. On the contrary, number of Arg-1 positive cells and Arg-1 fluorescence intensity in sham

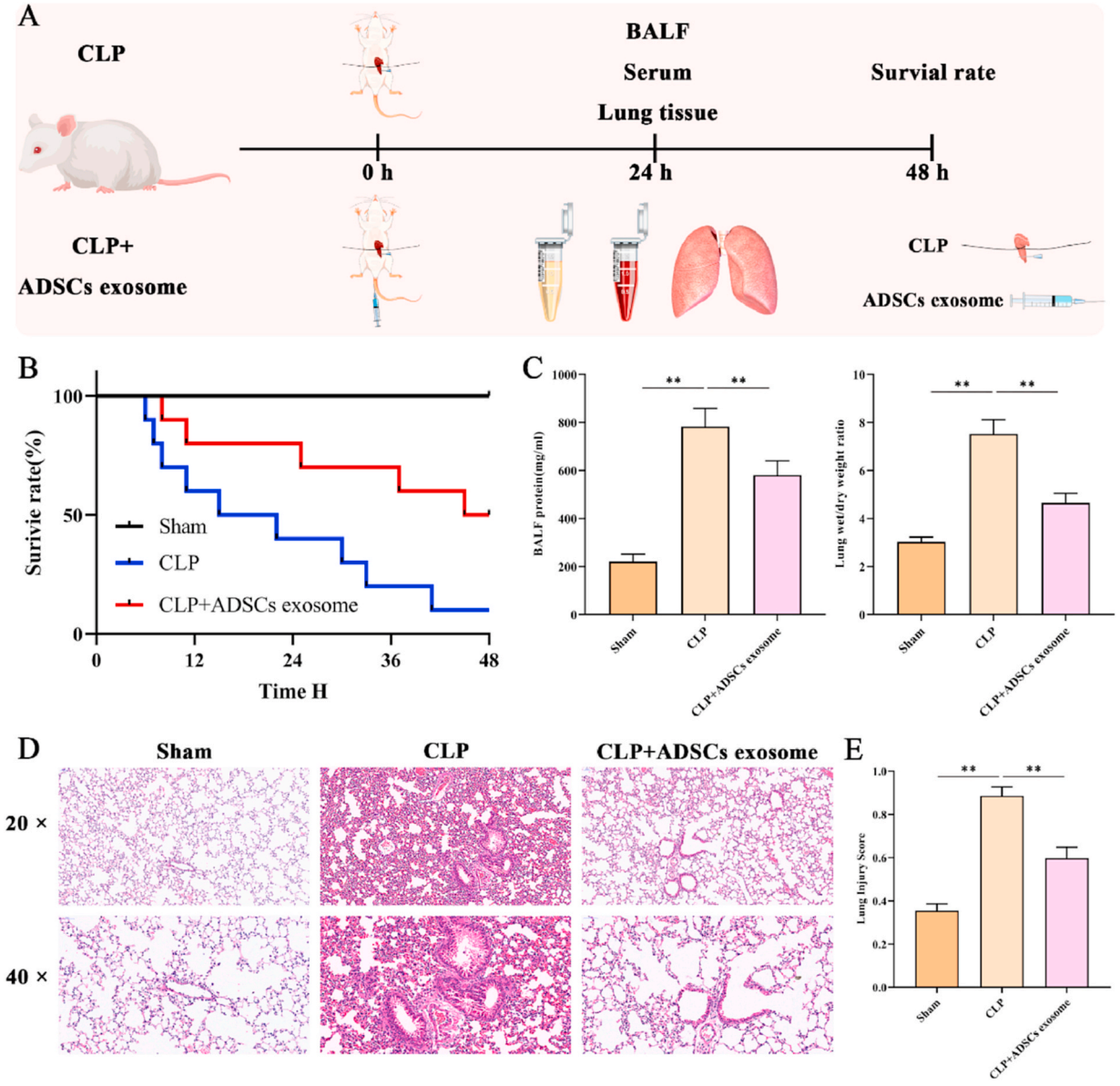

Fig. 8. ADSCs exosomes alleviated CLP induced acute lung injury in mice. A. Schematic illustration of animal experiments. B. Survivorship curve of CLP and ADSCs exosomes treated BALB/C mice. C. BALF protein content and wet/dry ratio of the mice lung tissue collected from CLP and ADSCs exosomes treated BALB/C mice. **: $P \leq 0.01$. D. HE results showing histology of the lung tissues in CLP and ADSCs exosomes treated BALB/C mice. Scale bar: 50 μm. E lung injury score of lung tissues in CLP and ADSCs exosomes treated BALB/C mice. **: $P \leq 0.01$.

and ADSCs exosome group was much more than that of CLP group (Fig. S2B). Besides, MPO immunohistochemical staining results indicated that MPO expression in neutrophils was significantly promoted in lung tissue of CLP induced sepsis mice, while ADSCs exosomes could bring the expression down (Fig. S2C). Above results indicated that ADSCs exosomes alleviated CLP induced inflammatory response in mice.

2.10. ADSCs exosomes alleviated CLP induced ROS and increased antioxidant ability in mice

Above results indicated that CLP induced inflammatory response and lung tissue damage in mice, while ADSCs exosome could alleviate CLP induced inflammatory response, improve lung tissue damage and reduce the death rate. Excessive ROS accumulation and impaired antioxidant ability are crucial reasons for lung injury in sepsis. To detect effect of CLP induced inflammatory response and ADSCs exosomes on oxidative stress and injury of pulmonary vascular endothelial cell, ROS, SOD, FRAP, MDA and GSH were detected. As Fig. 8A displayed, results indicated that ROS levels were remarkably elevated after CLP treatment, while ADSCs exosomes could reduce the accumulation. MDA detection indicated that level of MDA in the BALF of sepsis mice is much higher than that of sham group and ADSCs exosomes group (Fig. 9A). Meanwhile, level of antioxidant SOD, FRAP and GSH was significantly decreased when treated with CLP, while ADSCs exosomes could restore their contents. Tunel staining indicated that CLP increased apoptosis in mice lung tissue, while ADSCs exosomes mitigated apoptosis rat in sepsis lung tissue (Fig. 9B). 8OHdG and CD31 immunofluorescence double staining indicated that 8OHdG expression in CD31-positive cells were significantly higher in CLP group, while ADSCs exosomes group displayed reduced expression than CLP group (Fig. 9C).

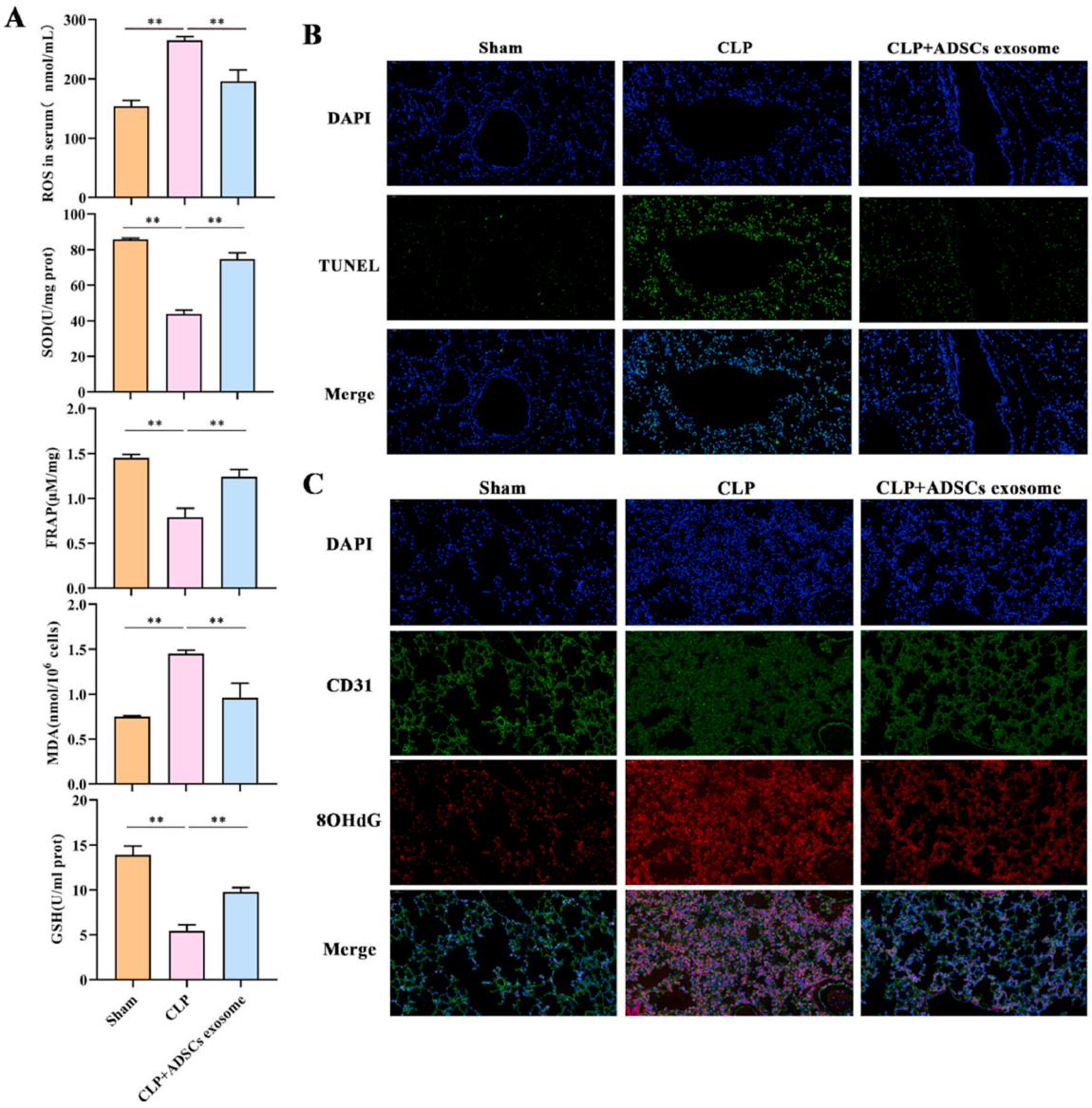

Fig. 9. ADSCs exosomes alleviated CLP induced ROS and increased antioxidant ability in mice. A. ROS, SOD, FRAP, MDA, and GSH content in the lung tissue in CLP and ADSCs exosomes treated BALB/C mice. **: $P \leq 0.01$. B. TUNEL immunofluorescent staining results in lung tissue of CLP and ADSCs exosomes treated BALB/C mice. Blue: DAPI; Green: TUNEL. C. CD31 and 8OHdG double immunofluorescent staining results in lung tissue of CLP and ADSCs exosomes treated BALB/C mice. Blue: DAPI; Green: CD31; Red: 8OHdG. (For interpretation of the references to colour in this figure legend, the reader is referred to the Web version of this article.)

2.11. ADSCs exosomes alleviated CLP induced ferroptosis via upregulating GPX4 in lung tissue

In cell experiments, our results revealed that ADSCs exosomes could alleviate inflammatory response induced PMVECs ferroptosis via upregulating GPX4. To verify the regulative effect of ADSCs exosomes on ferroptosis and GPX4 expression in CLP induced acute lung injury, expressions of 4HNE and GPX4 were detected via western blot, PCR and immunofluorescence staining. As is shown in Fig. 10A, western blot results indicated protein expression of 4HNE in lung tissue was significantly increased when treated with CLP, while the expression was greatly decreased with ADSCs exosomes. Just the opposite, the expression of GPX4 was downregulated when treated with CLP and upregulated when ADSCs exosomes were added. Interestingly, treatment with both CLP and ADSCs exosomes could increase expression of HO-1, while ADSCs exosomes increased HO-1 more than CLP (Fig. 10A). Immunohistochemical staining results of 4HNE, GPX4 and HO-1 also showed that CLP treatment increased 4HNE and HO-1 positive cells in lung tissue and decreased GPX4 positive cells (Fig. 10B). Meanwhile, ADSCs exosomes reduced number of 4HNE positive cells and increased numbers of GPX4 and HO-1 positive cells (Fig. 9B). Consistent with western blot and immunohistochemical results, PCR results showed same regulative effect of CLP and ADSCs exosomes on expression of HO-1 and GPX4 (Fig. 10C). Besides, 4HNE and GPX4 immunofluorescence staining results also indicated that CLP increased 4HNE expression and decreased GPX4 expression in lung tissue, while ADSCs exosomes increased GPX4 expression and decreased 4HNE expression (Fig. 10D). Hence, ADSCs exosomes alleviated CLP induced ferroptosis via upregulating GPX4 in lung tissue.

2.12. ADSCs exosomes regulated expression of Keap1/Nrf2 in CLP induced acute lung injury

Keap1/Nrf2 system is key element of oxidative stress system via

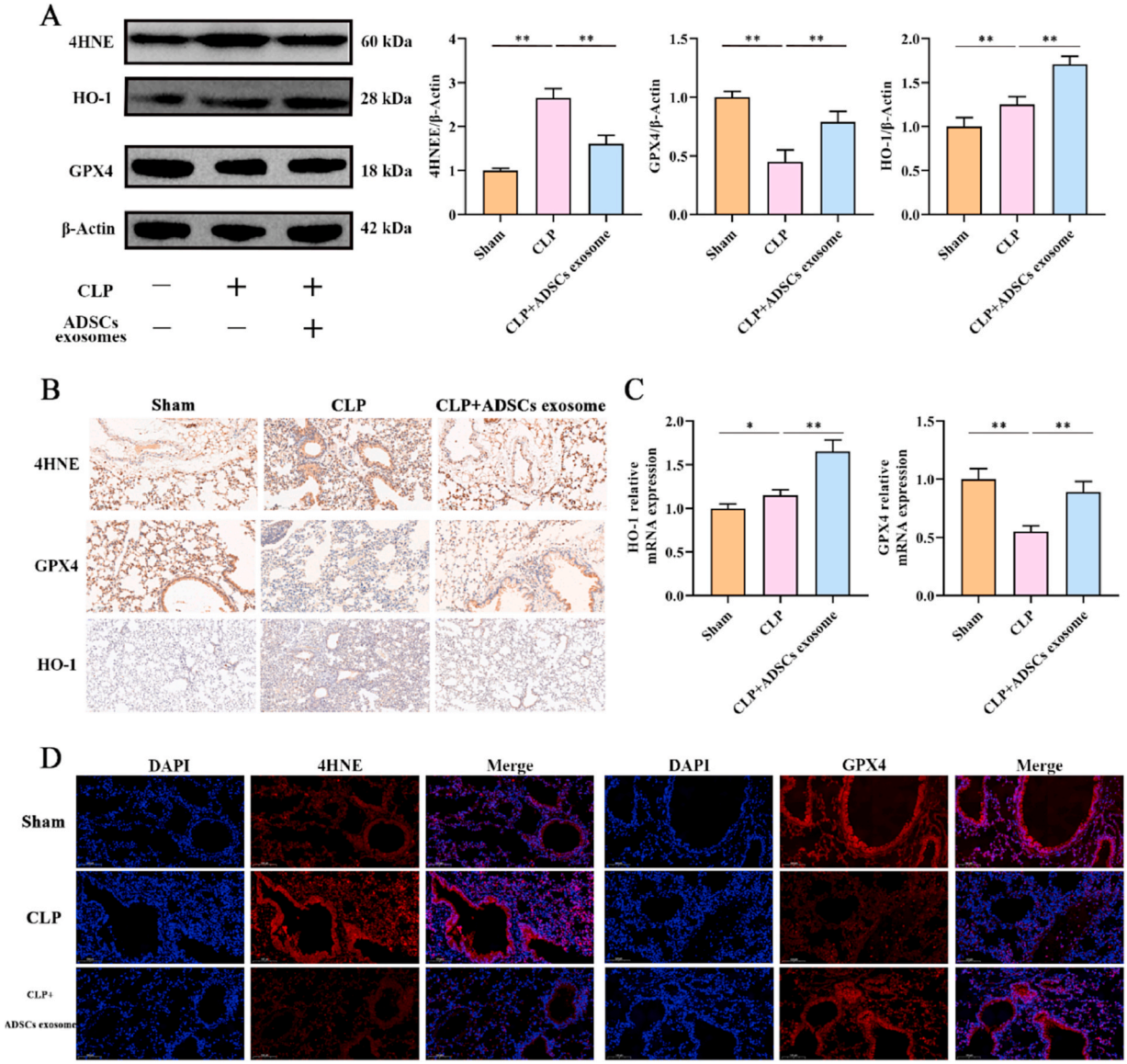

Fig. 10. ADSCs exosomes alleviated CLP induced ferroptosis via upregulating GPX4 in lung tissue. A. 4HNE, GPX4 and HO-1 expressions in lung tissue of CLP and ADSCs exosomes treated BALB/C mice detected by western blot, * *: P ≤ 0.01. B. 4HNE, GPX4 and HO-1 expressions in lung tissue of CLP and ADSCs exosomes treated BALB/C mice detected by 4HNE, GPX4 and HO-1immumohistochemical staining respectively. C. HO-1 and GPX4 mRNA expressions in lung tissue of CLP and ADSCs exosomes treated BALB/C mice detected by PCR. D. 4HNE (left) and GPX4(right) immunofluorescent staining results in lung tissue of CLP and ADSCs exosomes treated BALB/C mice, Blue: DAPI; Green: 4HNE (left), GPX4 (right). (For interpretation of the references to colour in this figure legend, the reader is referred to the Web version of this article.)

regulating a series of antioxidative gene, such as GPX4 and HO-1. Expression of key component in Nrf2 and Keap1 signaling pathway were also detected. As shown in Fig. 11A, protein expression of Nrf2 was slightly increased in CLP induced sepsis lung tissue, and remarkably increased in ADSCs exosomes treated mice. However, the expression of Keap1, negative regulator of Nrf2, was slightly decreased in CLP induced sepsis lung tissue, and remarkably decreased in ADSCs exosomes treated mice (Fig. 11A). PCR results also revealed increased Nrf2 mRNA expression in ADSCs exosomes treated sepsis mice lung tissue (Fig. 11A). Similarly, the expression of antioxidant molecules HO-1and GPX-4 was significantly upregulated when treated with ADSCs exosomes (Fig. 9B). Nrf2 and CD31 immunofluorescence double staining result also revealed

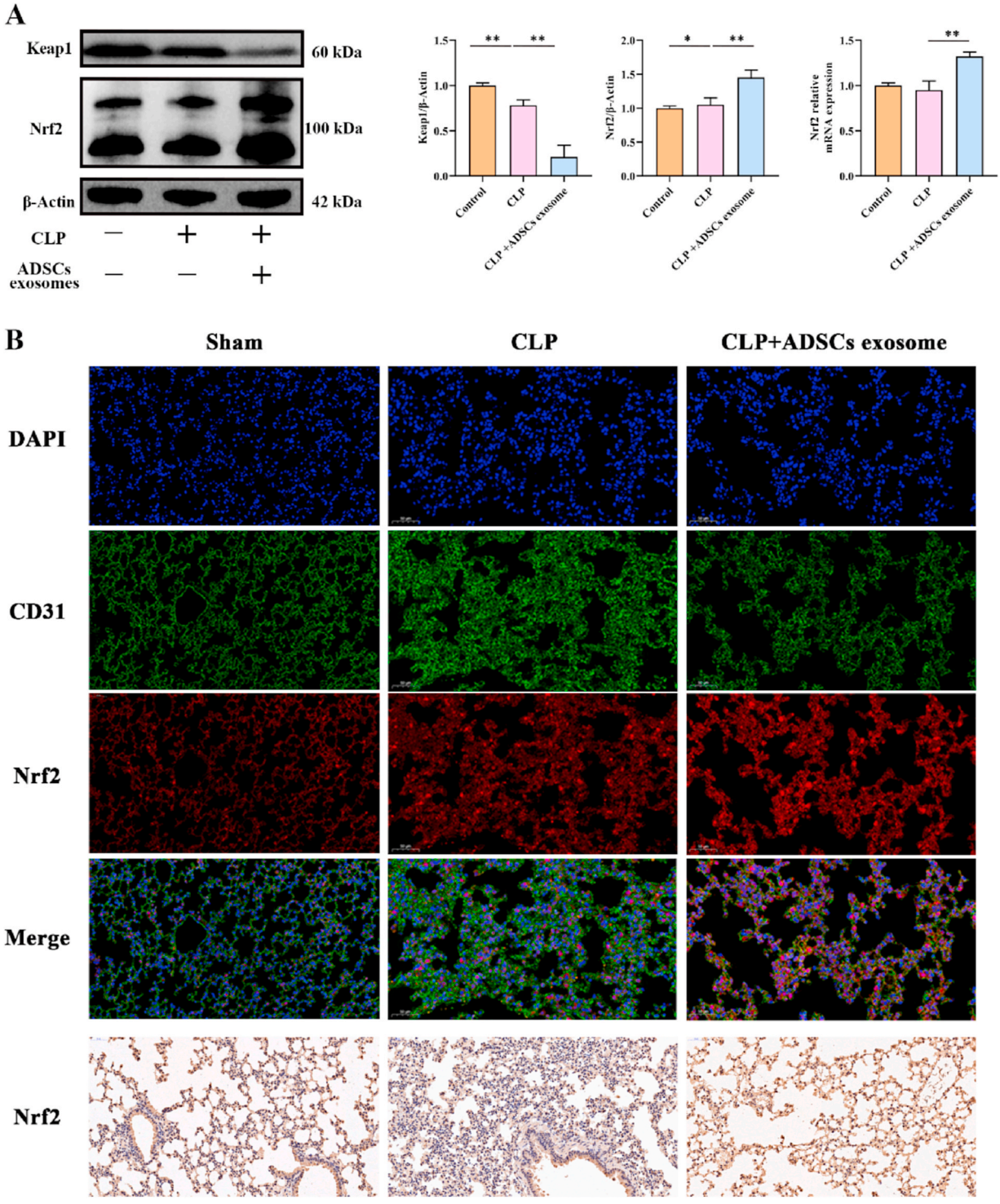

Fig. 11. ADSCs exosomes regulated expression of Keap1/Nrf2 in CLP induced acute lung injury. A. Nrf2 and Keap1 expressions in lung tissue of CLP and ADSCs exosomes treated BALB/C mice detected by western blot; Nrf2 RNA expressions in lung tissue of CLP and ADSCs exosomes treated BALB/C mice detected by PCR, * *: $P \leq 0.01$. B. Nrf2 and CD31 double immunofluorescent staining results in lung tissue of CLP and ADSCs exosomes treated BALB/C mice. Blue: DAPI; Green: CD31; Red: Nrf2. Nrf2 expressions in lung tissue of CLP and ADSCs exosomes treated BALB/C mice detected by Nrf2 immumohistochemical staining. (For interpretation of the references to colour in this figure legend, the reader is referred to the Web version of this article.)

that Nrf2 mean fluorescence intensity in $CD31^+$ cells were higher than $CD31^-$cells, and the intensity in ADSCs exosomes mice lung tissue was higher than that of CLP group (Fig. 11B). Besides, Nrf2 immunohistochemical staining results also indicated that this antioxidant molecules were slightly upregulated in CLP mice lung tissue, while significantly promoted when treated with ADSCs exosomes (Fig. 11B). Consequently, ADSCs exosomes regulated expression of Keap1/Nrf2 in CLP induced acute lung injury.

3. Discussion

Sepsis is defined as a life-threatening condition of multiorgan dysfunction resulting from a dysregulated host response to infection, which features excessive inflammatory response as a result of the uncontrolled release of inflammatory mediators [2,5,34]. Among all the complications induced by sepsis, acute lung injury is the earliest and most deadly one, mortality of which is as high as 60% [35,36]. Interestingly, interaction between activated AM and PMVECs plays an important role in the initiation of acute lung injury [8]. After severe infection and symptoms of sepsis occurs, pulmonary microvascular lesions, combined with recruited leukocytes, contribute to excessive inflammatory cytokines and ROS production [37]. Undue inflammatory cytokines storm and ROS production then damage PMVECs and the endothelial barrier [38]. Excessive inflammatory cytokines and ROS affects lipids, proteins, and DNA, and promotes irreversible oxidative stress in endothelial cells [39]. Furthermore, oxidative stress in endothelial cells enhances apoptosis and lead to increase of vascular permeability, resulting in more infiltration of inflammatory cell, and thus lead to worsen damage [40]. Consequently, it is of great significance to alleviate excessive inflammatory response and ROS accumulation and resultant PMVECs injury in the protection of sepsis induced acute lung injury. In this study, we found that the lung tissue was significantly damaged after CLP induced sepsis, exhibiting pulmonary edema, hemorrhage, and inflammatory cell infiltration. Lung injury assessment also indicated that sepsis would induce acute lung injury. And detection of inflammatory response and ROS production indicated that excessive ROS production and inflammatory response were involved in sepsis induced lung injury.

ADSCs exosomes, an important means of cellular communication, is a promising mediator in tissue repair and regeneration as well as regulation of inflammation [41–43]. It is no doubt that ADSCs exosomes can promote wound healing via regulating viability and function of fibroblast and vascular endothelial cell [25]. Emerging studies indicated that ADSCs exosomes can improve CLP induced organ damage through suppressing excessive inflammatory response [44,45]. Our previous researches indicated that ADSCs could alleviate CLP induced lung injury by suppressing expression M1 macrophage by Nrf2/HO-1 and Notch pathways [29]. As key mediators and victims of acute lung injury, both PMVECs and macrophages play an important role in acute lung injury. In this study, to verify whether ADSCs exosomes could alleviate PMVECs injury in sepsis, we designed cell damage model. Macrophages were stimulated with LPS to induce inflammatory response in vitro, and superstratum conditioned culture medium of which were collected to damage PMVECs. Results indicated that CM of macrophage damaged PMVECs, cell viability proliferation and migration of which were weaken while apoptosis increased. Specifically, ROS accumulation as well as decrease of antioxidant ability were observed in inflammation induced PMVECs injury. Interestingly, signs of ferroptosis were also observed in inflammation induced PMVECs injury. Of note, ferroptosis is not synonymous with generalized production of ROS; indeed, it can be ROS production without ferroptosis, but ferroptosis generally involves the oxidation of specific lipids rather than generalized accumulation of ROS.

Ferroptosis, a unique form of cell death featuring iron-dependent phospholipid peroxidation, was identified as a distinct phenomenon and named a decade ago [46]. Ferroptosis is regulated by multiple cellular metabolic pathways, such as redox homeostasis, iron handling, mitochondrial activity and metabolism of amino acids, lipids and sugars [11]. Although the specific cellular and molecular pathophysiological mechanisms triggering ferroptosis and the mechanisms by which ferroptosis triggers cause pathological sequelae are in many cases not known, ferroptosis has been implicated in a broad set of biological contexts as well as many pathological, from development to aging, immunity, and cancer [46–48]. Ferroptosis has been implicated in the response to infectious agents [49]. Numerous viruses influence host iron metabolism, iron transport, ROS production, and antioxidant defenses. Severe acute respiratory syndrome coronavirus 2 (SARS-CoV-2) may activate ferroptosis during infection [50]. Patients with COVID-19 have high serum ferritin levels, suggesting high iron exposure in tissues. HCV model and other models have been reported over the past decade in which ferroptosis is activated during organ injury [11]. It's worth noting that the vascular leakage that occurs during sepsis, which can result in injury of multiple organs, is associated with gene expression, metabolomic changes, and markers characteristic of ferroptosis. In this study, we reveled that ferroptosis participated in inflammation induced PMVECs injury in sepsis induced lung injury. Specifically speaking, expression of GPX4 in PMVECs was significantly decreased when treated with CLP (in vivo) and LPS stimulated macrophage CM (in vitro). On the contrary, expressions of lipid peroxidation marks in PMVECs, including MDA and 4HNE, were significantly boosted when exposed to excessive inflammation. And interestingly, ADSCs exosomes alleviated excessive inflammation induced PMVECs ferroptosis, accounting for protective effect of ADSCs exosomes in sepsis induced acute lung injury. And we the first to reveal that ADSCs exosomes protect PMVECs from excessive inflammation induce injury via suppressing ferroptosis in sepsis induced acute lung injury. This study identified that excessive inflammation response is one of the diverse triggers for ferroptosis and shed light on the mechanisms and contexts in which this form of cell death is activated pathologically in sepsis induced acute lung injury.

To further elucidate specific mechanism that how ADSCs inhibit inflammation induced PMVECs ferroptosis, regulative effect of ADSCs exosomes on GPX4 and Nrf2 were conducted. There are certain crucial control points that can potently and selectively suppress ferroptosis. The process of ferroptosis is driven by the peroxidation of specific lipids, and upregulation of GPX4 is a direct means of intervening in ferroptosis. GPX4 is a selenoprotein that functions as a GSH-dependent peroxidase to counter the oxidation of lipids in membranes [22]. GSH depletion reduces the activity of GPX4, which is a key event upstream of mitochondrial dysfunction, leading to ferroptosis [20]. Hence, reduction of GPX4 activity is taken as signs of ferroptosis and attempts to restore expression and activity of GPX4 are important strategies to suppress ferroptosis. In this study, we found that ADSCs exosomes could restore excessive inflammation induced GPX4 suppression. Besides, when expression of GPX4 was inhibited by RSL3, suppression of ADSCs exosomes on excessive inflammation induced ferroptosis was counteracted. Nrf2,is a crucial transcription factor, functioning as an intracellular defense mechanism to counteract oxidative stress via coordinating the activation of several cytoprotective genes encoding cytoprotective and antioxidative enzymes. Under normal conditions, Nrf2 combines with its negative regulator, Keap1, in the cytoplasm, where it is degraded rapidly through ubiquitination. In response to oxidative stress, Nrf2 dissociates from Keap1 and translocates into the nucleus and transactivates the genes containing the antioxidant response element (ARE) in their promoters, such as GPX4 and HO-1 [29,51]. Recent studies including our previous study reported that MSC-Exo ameliorated oxidative stress-induced injury by regulating the Nrf2 and its downstream antioxidative genes [52,53]. This study also revealed that ADSCs exosomes could regulate expression of GPX4 via targeting Keap1, the regulator of Nrf2, and thus increase expression of Nrf2 and GPX4 in inflammation damaged PMVECs. These results indicated that ADSCs exosomes inhibited PMVECs ferroptosis by upregulating GPX4 expression via repressing Keap1 and promoting Nrf2 expression and translocation into

nucleus. And these findings help to elucidate the full array of initiating mechanisms for ferroptosis and the contexts in which they are used, which greatly enrich our understanding of how ferroptosis fits into the broader world of biology and medicine.

MicroRNA is a kind of key non-coding RNA (ncRNAs), 18-22 nt, which mainly bind to gene's 3′UTR and regulate their expression [54]. Although there are emerging studies indicating that ADSCs exosomes contain a variety of signaling molecules such as phosphatidylcholine and sphingosine-1-phosphate, it's worth noting that miRNA contents are relatively high in exosome compared with other components (protein, mRNA, lipid and DNA), for exosomes would protect miRNAs from degradation [43]. Consequently, abundant miRNA contents grant exosomes multiple regulative effect on recipient cells. However, miRNA expression profile in exosomes from different cells differ from one another [55]. For example, exosomes from stem cells are different from that of non-stem cells, exosomes from morbid state are different from that of health, and exosomes from senescent cells is different from that of young cells. In this study, to find out what kind of miRNA regulate Keap1 pathways, we conducted miRNA microarray and drew expression profile of ADSCs exosomes. Further bioinformatics analysis indicated that miR-125b-5p may be a regulator of Keap1. Via dual luciferase reporter assay, miR-125b-5p mimic and inhibitor transfection and inhibition of exosomes miR-125b-5p, we proved that ADSCs exosomes relieved inflammation induced PMVECs ferroptosis and protected lung injury from sepsis via specific delivery of miR-125b-5p and regulation of Keap1. By literature review, we noticed that several miRNAs, such as miR21, miR125b, let7, and miR24, were enriched in a series of MSCs, including ADSCs, UCB-MSCS and BMSC [56,57]. And the contents of these miRNAs are quiet low in non-stem cells and morbid cells, which possibly account for therapeutical effect of stem cell exosomes [58]. However, different research enrolled different exosomes samples, making it hard to conduct horizontal comparison, which is also one of the limitations of this study. So, more efforts should be devoted to this filed and distinguish difference in exosomes from different cells and illustrate the mechanism underlying it.

4. Conclusion

In this study, we found that LPS stimulated macrophage CM induced PMVECs injury and increased ferroptosis, while ADSCs exosomes could alleviate the injury and decrease ferroptosis. Besides, ADSCs exosome upregulated expression of GPX4 in LPS stimulated macrophage CM treated PMVECs. And further GPX4 inhibition experiments revealed that ADSCs exosomes alleviated inflammatory response induced ferroptosis via upregulating GPX4 in PMVECs. Meanwhile, ADSCs exosomes could increase the expression and nucleus translocation of Nrf2 which acts as the regulator of GPX4, while decrease the expression of Keap1, a negative regulator of Nrf2. What is more, miRNA analysis indicated that miR-125b-5p enrichment in ADSCs exosomes suppressed expression of Keap1 and alleviated ferroptosis. And in CLP induced sepsis model, ADSCs exosomes could relieve the oxidative stress injury and ferroptosis of lung tissue, while remarkably increase expression of Nrf2 and GPX4. Collectively, we illustrated a novel potentially therapeutic mechanism that miR-125b-5p delivery by ADSCs exosomes could alleviate the inflammation induced PMVECs ferroptosis in sepsis induce acute lung injury via regulating Keap1/Nrf2/GPX4 expression, hence improve the acute lung injury in sepsis.

5. Methods and materials

5.1. Preparation of ADSCs

Adipose tissues were collected from patients receiving abdominal liposuction surgery at Department of Burns and Cutaneous Surgery, Xijing Hospital under approved guidelines (BSH [2015] D-15). The age of volunteer patients ranged from 19 to 29 years old. Informed consent of the purpose and procedure of this study were given to volunteer patients. And all patients provided written informed consent to participate. ADSCs were isolated as our previous protocol [29,30]. After washed in sterile phosphate buffer saline (PBS) containing 1% Penicillin-Streptomycin, the adipose tissue was cut into 1-mm pieces. Then, the fragmented tissue was digested with 1 mg/ml collagenase type I (Sigma, C1-BIOC, USA) for 60 min at 37 °C. Digested tissues were filtered through a 100-μm mesh and centrifuged at 300 g for 5 min. After washing with PBS, the cells were transplanted into the 25 cm^2 plate with human ADSCs culture medium (Cyagen Biosciences, HUXMD-90011, China) supplemented with 10% FBS, 100 U/ml penicillin, and 100 μg/ml streptomycin. The cells were cultured at 37 °C in humid air with 5% CO_2. 24 h after seeding to the plate, culture medium of the cells was replaced. The morphology of cells was observed with inverted phase contrast microscope, and passaged every 3–4 days thereafter. For cell characterization, the surface molecule CD29, CD34, CD44, CD45, CD73, CD90 expression profiles of extracted ADSCs (P3) were detected by flow cytometry (BD FACS Calibur™, Becton-Dickinson, San Jose, CA, USA).

5.2. Exosome isolation and characterization

ADSCs P3 to P5 were cultured in T-225 flask and cultured until 80% confluence with human ADSCs culture medium supplemented with 10% FBS, 100 U/ml penicillin, and 100 μg/ml streptomycin. After washing cells twice with PBS, human ADSCs culture medium without FBS was added to the flask, and the cells were cultured for 24 h. Conditioned culture medium were collected for exosomes isolation with differential ultracentrifugation as previously described [29]. Extracted exosomes were resuspended in PBS and stored at−80 °C for characterization and further use. Morphology of the isolated vesicles was observed by transmission electron microscopy (TEM). And particle size distribution and concentration of exosomes were analyzed with Nanoparticle Tracking Analysis (NTA). The protein markers, CD9, CD63, and TSG101 expressions of extracted vesicles were detected by western blot. Extracted ADSCs exosomes were labeled with PKH26 (Sigma, PKH26PCL, USA), added into PMEVCs for 12 h and observed with laser scanning confocal microscope.

5.3. PMEVCs isolation and culture

As previously described, primary PMVECs were isolated from lung tissues in healthy newborn BALB/c mice [8]. Fresh BALB/c mice lung tissue were isolated and washed with 100 mL of PBS. The pleura was carefully cut away, and the outer edges of the remaining lung tissue with no large blood vessels were harvested, and the lungs were again rinsed in PBS. The tissues were cut into pieces, placed in a flask (Costar, Corning, NY), and cultured in an endothelial cell medium (ECM) (Sciencell, San Diego, CA). The ECM consists of a basal medium, an endothelial cell growth supplement, a penicillin/streptomycin solution, and a low concentration of fetal bovine serum (FBS; 5%). The tissue cultures were incubated in a humidified incubator at 37 °C with a 5% CO_2 atmosphere. After 60 h, the tissues were removed, and the culture medium was replaced every 2 days thereafter. After confluence, the cells were harvested by treatment with a 0.25% solution of trypsin. Cell isolates were characterized by cobblestone morphology and immunofluorescence staining for CD31. Cells from passages 3–5 were studied.

5.4. RAW264.7 culture and treatment

The RAW264.7 cells were purchased from American Type Culture Collection (ATCC), and cultured in RPMI 1640 medium containing 10% fetal bovine serum (FBS), 100 U/ml penicillin, and 100 μg/ml streptomycin. 100 ng/mL Lipopolysaccharide (LPS, Sigma–Aldrich) was added to RAW264.7 cells for 12 h to induce M1 polarization. The concentration of inflammatory cytokines (IL-1β and TNF-α) in the media was measured with an enzyme-linked immunosorbent assay kit (Abcam) following the

protocols provided. Then, LPS stimulated RAW264.7 cells medium were added to PMEVCs to induce oxidative stress injury, while 30 μg/mL ADSCs exosomes were added to verify its protective effects. After 12 h incubation, cells and culture medium were collected for further detection.

5.5. PMEVCs treatment and detection

PMEVCs (P3-P5) were seeded into 6 well plate, and treated with LPS stimulated macrophage conditioned medium and ADSCs exosomes. 24 h after the treatment, CCK8 were used to test the cell viability of PMEVCs following the protocol provided. Apoptosis was detected by flow cytometry using an Annexin V- and propidium iodide staining kit (BD Pharmingen™, Cat: 556547, USA) according to the manufacturer's instructions as well as caspase3 western blot.

5.6. PMEVCs migration, and tube formation assays

PMEVCs migration and tube formation ability were detected via transwell as well as scratch assay and tubule formation assay. For scratch assay, PMEVCs were seeded at 6 well plate with 1×10^6 cells/well. After treatment of LPS stimulated macrophage conditioned medium and ADSCs exosomes for 24 h, a 10 μL pipette tip was used to induce a scratch. Wound closure was observed and photographed at 0 h, 12 h, 24 h, and 48 h by the FSX100 microscope (Olympus, Tokyo, Japan). For transwell assay, differently treated PMEVCs were seeded into upper chamber of transwell with DMEM without FBS, while DMEM with 10% FBS in the 24 well plate. 12 h after treatment, upper chamber was fixed with 4% paraformaldehyde, stained with crystal violet observed and photographed by the FSX100 microscope (Olympus, Tokyo, Japan). For tube formation assays previously treated PMVECs were seeded in a 24-well plate coated with 200 μL Matrigel (BD Biosciences, Bedford, MA, USA) per well. After incubated at 37 °C for 12 h, tube formation was observed and photographed by the FSX100 microscope (Olympus, Tokyo, Japan).

5.7. ROS and antioxidative activities of PMEVCs

ROS production was detected, based on the oxidation of 7-dichlorodihydrofluorescein diacetate (DCFH-DA) to 2,7-dichlorodihydrofluorescein, with a ROS detection kit (Boster, China) following manufacture' instruction. DNA damage was observed via 8OHdG immunofluorescence staining. Mitochondrial membrane potential (MMP) in PMEVCs were detected by JC-1 staining (M8650, Solarbio, Beijing, China) according to the manufacturer's instructions. Culture medium supernatant were collected by centrifugation at 12,000×*g* for 5 min to measure antioxidant activity, including ferric ion reducing antioxidant power (FRAP) (A015-3, Nanjing Jiancheng Bioengineering Institute, China), GSH (A005, Nanjing Jiancheng Bioengineering Institute), or SOD (A001-3, Nanjing Jiancheng Bioengineering Institute) according to the manufacturer's instructions. Each determination was made the average of at least three independent experiments.

5.8. Lipid ROS of PMEVCs

For cell experiments, Lipid ROS in PMEVCs were detected by C11 BODIPY staining, MDA kit and 4HNE expression (western blot). For animal experiments, lipid ROS were detected by staining, MDA kit and 4HNE expression (western blot, immunofluorescent and immunohistochemical staining). C11 BODIPY staining were conducted as manufacture' instruction and observed with laser scanning confocal microscope. MDA contents were detected by MDA kit according to the manufacturer's instructions. And 4HNE expression were detected via western blot, immunofluorescent and immunohistochemical staining as previously described.

5.9. Transient transfection

PMEVCs cells were transfected with miR-125b-5p mimic and inhibitor using lipofectamine 2000 reagent according to the manufacturer's directions, with non-specific siRNA (NSsiRNA) as control. In brief, the PMEVCs were seeded into 6-well plates and incubated with mimic and inhibitor or NSsiRNA for 24–48 h in serum-free medium. Transfection efficiency was measured at 24, 48 h after transfection by RT-PCR and western blot. Stable transfections were used in further experiment.

To inhibit miR-125b-5p expression in ADSCs exosomes, inhibitor of miR-125b-5p were transferred into ADSCs exosomes with ExoLoad kit (Cat#ELSR-06, ECHO-biotech, Beijing China) following the instructions. Briefly, 100 μL(1 mg/mL) ADSCs exosomes were incubated with 1000 pmol(50 μL) miR-125b-5p inhibitor and 200 μL ETP at 37 °C with 150 rpm vibrating. After 2 h incubation, exosomes were condensed with 100 kDa ultrafiltration at 4000 g to a volume of 100 μL. After washing with washing buffer for 2 times, exosomes were collected for miR-125b-5p expression analysis and further experiments.

5.10. sRNA sequencing and analysis

Small RNAs contained in ADSCs exosomes were determined by Illumina HiSeq (Majorbio, Shanghai, China). In brief, RNA in isolated ADSCs exosomes was extracted using the Exosomal RNA Isolation Kit (Norgen) according to the manufacturer's instructions. The quality of RNA was determined by A260/280. Small RNA adapters were then ligated to the 5′ and 3′ ends of total RNA. After cDNA synthesis and amplification, the PCR-amplified fragments were purified from the PAGE gel, and the completed cDNA libraries were quantified by the Agilent Bioanalyzer 2100 system using DNA High Sensitivity Chips. Cluster generation was performed on an Illumina cBot, and sequencing was performed on an Illumina HiSeq 2000 according to the manufacturer's instructions. The miRDB, miRtarbase, starBase and TargetScan database were used to predict the genes targeted by the differentially expressed miRNAs. Functional enrichment of GO (GeneOntology) terms and KEEG (Kyoto Encyclopedia of Genes and Genomes) analyses were then performed to annotate these differentially expressed miRNA targets.

5.11. Dual-luciferase reporter assay

Luciferase vectors containing wild-type or mutant 3'-UTR of Keap1 and miR125b-5p mimics or miR-Control were constructed by HANBIO (Shanghai, China). And cells were co-transfected with luciferase vectors using Lipofectamine 3000 (Invitrogen). Luciferase activity was measured using a Dual-Luciferase Reporter Assay System (Beyotime) after 48 h transfection.

5.12. Animal models

Six-to eight-week-old male healthy BALB/C mice were brought from Experimental Animal Centre of Air Force Military University (Xi'an, China). Mice were maintained under standard conditions with free access to food and water. All animal procedures were performed in accordance with the Guide for the Care and Use of Laboratory Animals (8th edition, 2011) and approved by the Institutional Animal Care and Use Committee of the Air Force Military University. Cecal ligation and puncture (CLP) was conducted to induce sepsis as previously described [59]. Sham group received the same procedure expect for CLP. Tail intravenous injection of 100 μg ADSCs exosomes to each mouse for resuscitation was conducted, while control group received isovolumetric PBS without ADSCs exosomes. 24 h after operation, the mice were sacrificed to obtain serum, lung, liver, heart, spleen, and kidney samples for antioxidant activity measurement and histological observation.

5.13. Western blot

Expression of Nrf2, HO-1, GPX4 and 4HNE were detected by western blot. Tissue samples were smashed with a homogenizer. Protein from cell and tissue samples were extracted and conducted with western blot as previously described. The concentrations were detected by BCA kit. The protein samples were separated by electrophoresis in a 10% polyacrylamide gel and transferred onto PVDF membranes. Then the membranes were blocked in 5% non-fat dried milk with Tris-buffered solution containing 0.1% Tween-20 (TBST) at room temperature for 1 h. Nrf2, HO-1, GPX4, 4HNE and β-Actin, were detected and visualized with ECL. ImageJ was used to quantify densities of the bands, while GraphPad Prism was used for graphs.

5.14. ELISA detection

Serum levels of ROS, IL-1β, and TNF-α were determined by ELISA using commercially available kits from R&D Systems, Inc., Minneapolis, MN.

5.15. Lung injury measurement

The entire lungs were collected for lung wet/dry ratio (W/D) measurement to assess pulmonary edema after the mice were sacrificed 24 h after CLP. Bronchoalveolar lavage was performed by injecting the lungs with 0.9% saline (0.5 mL) through the main bronchus, and this procedure was repeated three times. The BALF was centrifuged for 10 min at 1200 rpm. The supernatants were collected and stored at −80 °C. Protein concentrations in BALF were determined by a protein detection kit.

5.16. Hematoxylin-eosin staining

Collected mouse tissue samples were fixed in 4% paraformaldehyde, dehydrated, embedded, cut into 5-μm-thick sections and mounted. The sections were stained with hematoxylin–eosin (H&E) and observed under an FSX100 microscope (Olympus).

5.17. Immunofluorescence analysis

PKH26 labeled ADSCs exosomes were added into PMVECs. After coculture for 12 h, the PMVECs were stained with DAPI (Bio-rad). Immunofluorescence signals were visualized with secondary antibodies by FSX100 microscope (Olympus). The 8OHdG immunofluorescence analysis was performed to assess DNA damage of PMVECs in CLP treated mice as described previously. To identify DNA damage in PMVECs, lung tissues were detected using monoclonal mouse DAPI (Bio-rad), CD31 (Bio-rad), 8OHdG (Abcam), HO-1(CST), 4HNE(Bioss), GPX4 (Abmart) and Nrf2(Abmart) antibodies according to manufacturer's instructions. Immunofluorescence signals were visualized with secondary antibodies by FSX100 microscope (Olympus).

5.18. Flow cytometry

PMVEC apoptosis was measured by flow cytometry using an Annexin V- and propidium iodide staining kit (BD Pharmingen™, Cat: 556547, USA) according to the manufacturer's instructions. The level of intracellular ROS in PMVECs was measured by 2′,7′-dichlorofluorescein (DCFH-DA) (Beyotime, S0033, China) following the recommended protocols. Analyses were performed with flow cytometry (BD FACSAria™ III system, USA). Levels of intracellular ROS were quantified by the mean fluorescent intensity (MFI).

5.19. Statistical analysis

A total of three independent experiments were performed for all analyses. All data are presented as the mean ± SD. Statistical comparisons among groups (≥3) were analyzed using a one-way ANOVA and the Student–Newman–Keuls q test (Graph Pad Prism 8.0), while comparisons among groups (=2) were analyzed by a T test (Graph Pad Prism 8.0). Differences with $P < 0.05$ were considered statistically significant.

Ethics approval and consent to participate

All animal studies were approved by the Animal Care and Use Committee of Fourth Military Medical University, and all experimental protocols were approved by the Medical and Ethics Committee of Xijing Hospital, Fourth Military Medical University, Xian, China.

Funding

This work was supported by grants from the National Natural Science Foundation of China, China (82172210 and 82272261) and the Key Research and Development Program of Shaanxi Province, China (2022SF-047 and 2023-ZDLSF-24).

Author contributions

Conceptualization, Dadai Hu and Yunchuan Wang.
Methodology (animal model), Xujie Wang and Jin Li;
Investigation, Kuo Shen and Weixia Cai;
Validation, Shaohui Li, Ruizhi Wang and Hao Zhang;
Data Curation, Yanhui Jia and Lixia Zhang;
Writing – Original Draft Preparation, Kuo Shen and Yunwei Wang;
Writing – Review & Editing, Yunchuan Wang and Dahai Hu;
Visualization, Yuxi Chen and Yuting Du;
Supervision, Yunchuan Wang and Xuekang Yang;
Project Administration Dadai Hu;
Funding Acquisition, Xuekang Yang, Yunchuan Wang and Dahai Hu.

Research support

This research received no external financial or non-financial support.

Consent for publication

All authors approved the submission of the manuscript to this journal.

Relationships

There are no additional relationships to disclose.

Patents and intellectual property

There are no patents to disclose.

Other activities

There are no additional activities to disclose.

Declaration of compeitng interest

The authors declare no conflicts of interest.

Data availability

Data will be made available on request.

Acknowledgments

The authors thank all the other members in their laboratory for their

insight and technical support.

Appendix A. Supplementary data

Supplementary data to this article can be found online at https://doi.org/10.1016/j.redox.2023.102655.

References

[1] J.D. Baghdadi, R.H. Brook, D.Z. Uslan, et al., Association of a care bundle for early sepsis management with mortality among patients with hospital-onset or community-onset sepsis, JAMA Intern. Med. 180 (5) (2020) 707–716.
[2] K.E. Rudd, S.C. Johnson, K.M. Agesa, et al., Global, regional, and national sepsis incidence and mortality, 1990-2017: analysis for the Global Burden of Disease Study, Lancet 395 (10219) (2020) 200–211.
[3] Surviving sepsis campaign international guidelines, Pediatrics 145 (5) (2020).
[4] D. Liu, S.Y. Huang, J.H. Sun, et al., Sepsis-induced immunosuppression: mechanisms, diagnosis and current treatment options, Mil Med Res 9 (1) (2022) 56.
[5] T. van der Poll, M. Shankar-Hari, W.J. Wiersinga, The immunology of sepsis, Immunity 54 (11) (2021) 2450–2464.
[6] P. Luo, Q. Zhang, T.Y. Zhong, et al., Celastrol mitigates inflammation in sepsis by inhibiting the PKM2-dependent Warburg effect, Mil Med Res 9 (1) (2022) 22.
[7] R. Chen, C. Cao, H. Liu, et al., Macrophage Sprouty4 deficiency diminishes sepsis-induced acute lung injury in mice, Redox Biol. 58 (2022), 102513.
[8] W. Cai, K. Shen, P. Ji, et al., The Notch pathway attenuates burn-induced acute lung injury in rats by repressing reactive oxygen species, Burns Trauma 10 (2022), tkac008.
[9] Q. Lu, S. Huang, X. Meng, et al., Mechanism of phosgene-induced acute lung injury and treatment strategy, Int. J. Mol. Sci. 22 (20) (2021).
[10] T. Hirschhorn, B.R. Stockwell, The development of the concept of ferroptosis, Free Radic. Biol. Med. 133 (2019) 130–143.
[11] B.R. Stockwell, Ferroptosis turns 10: emerging mechanisms, physiological functions, and therapeutic applications, Cell 185 (14) (2022) 2401–2421.
[12] B. Hassannia, P. Vandenabeele, T. Vanden Berghe, Targeting ferroptosis to iron out cancer, Cancer Cell 35 (6) (2019) 830–849.
[13] B.R. Stockwell, A powerful cell-protection system prevents cell death by ferroptosis, Nature 575 (7784) (2019) 597–598.
[14] L. Wu, X. Tian, H. Zuo, et al., miR-124-3p delivered by exosomes from heme oxygenase-1 modified bone marrow mesenchymal stem cells inhibits ferroptosis to attenuate ischemia-reperfusion injury in steatotic grafts, J. Nanobiotechnol. 20 (1) (2022) 196.
[15] W. Xu, H. Deng, S. Hu, et al., Role of ferroptosis in lung diseases, J. Inflamm. Res. 14 (2021) 2079–2090.
[16] L. Shen, D. Lin, X. Li, et al., Ferroptosis in acute central nervous system injuries: the future direction? Front. Cell Dev. Biol. 8 (2020) 594.
[17] S. Van Coillie, E. Van San, I. Goetschalckx, et al., Targeting ferroptosis protects against experimental (multi)organ dysfunction and death, Nat. Commun. 13 (1) (2022) 1046.
[18] Y. Li, Y. Cao, J. Xiao, et al., Inhibitor of apoptosis-stimulating protein of p53 inhibits ferroptosis and alleviates intestinal ischemia/reperfusion-induced acute lung injury, Cell Death Differ. 27 (9) (2020) 2635–2650.
[19] H. Dong, Z. Qiang, D. Chai, et al., Nrf2 inhibits ferroptosis and protects against acute lung injury due to intestinal ischemia reperfusion via regulating SLC7A11 and HO-1, Aging (Albany NY) 12 (13) (2020) 12943–12959.
[20] F. Ursini, M. Maiorino, Lipid peroxidation and ferroptosis: the role of GSH and GPx4, Free Radic. Biol. Med. 152 (2020) 175–185.
[21] K. Bersuker, J.M. Hendricks, Z. Li, et al., The CoQ oxidoreductase FSP1 acts parallel to GPX4 to inhibit ferroptosis, Nature 575 (7784) (2019) 688–692.
[22] T.M. Seibt, B. Proneth, M. Conrad, Role of GPX4 in ferroptosis and its pharmacological implication, Free Radic. Biol. Med. 133 (2019) 144–152.
[23] M. Dodson, R. Castro-Portuguez, D.D. Zhang, NRF2 plays a critical role in mitigating lipid peroxidation and ferroptosis, Redox Biol. 23 (2019), 101107.
[24] Y. Li, J. Zhang, J. Shi, et al., Exosomes derived from human adipose mesenchymal stem cells attenuate hypertrophic scar fibrosis by miR-192-5p/IL-17RA/Smad axis, Stem Cell Res. Ther. 12 (1) (2021) 221.
[25] Y. Zhang, X. Bai, K. Shen, et al., Exosomes derived from adipose mesenchymal stem cells promote diabetic chronic wound healing through SIRT3/SOD2, Cells 11 (16) (2022).
[26] X. Bai, J. Li, L. Li, et al., Extracellular vesicles from adipose tissue-derived stem cells affect notch-miR148a-3p Axis to regulate polarization of macrophages and alleviate sepsis in mice, Front. Immunol. 11 (2020) 1391.
[27] Q. Yu, D. Wang, X. Wen, et al., Adipose-derived exosomes protect the pulmonary endothelial barrier in ventilator-induced lung injury by inhibiting the TRPV4/Ca(2+) signaling pathway, Am. J. Physiol. Lung Cell Mol. Physiol. 318 (4) (2020) L723–l741.
[28] H. Zhao, Q. Shang, Z. Pan, et al., Exosomes from adipose-derived stem cells attenuate adipose inflammation and obesity through polarizing M2 macrophages and beiging in white adipose tissue, Diabetes 67 (2) (2018) 235–247.
[29] K. Shen, Y. Jia, X. Wang, et al., Exosomes from adipose-derived stem cells alleviate the inflammation and oxidative stress via regulating Nrf2/HO-1 axis in macrophages, Free Radic. Biol. Med. 165 (2021) 54–66.
[30] M. Liu, Y. Yang, B. Zhao, et al., Exosomes derived from adipose-derived mesenchymal stem cells ameliorate radiation-induced brain injury by activating the SIRT1 pathway, Front. Cell Dev. Biol. 9 (2021), 693782.
[31] T. Bai, M. Li, Y. Liu, et al., Inhibition of ferroptosis alleviates atherosclerosis through attenuating lipid peroxidation and endothelial dysfunction in mouse aortic endothelial cell, Free Radic. Biol. Med. 160 (2020) 92–102.
[32] Y. Guo, S. Yu, C. Zhang, et al., Epigenetic regulation of Keap1-Nrf2 signaling, Free Radic. Biol. Med. 88 (Pt B) (2015) 337–349.
[33] S. Saha, B. Buttari, E. Panieri, et al., An overview of Nrf2 signaling pathway and its role in inflammation, Molecules 25 (22) (2020).
[34] J.L. Vincent, S.M. Opal, J.C. Marshall, et al., Sepsis definitions: time for change, Lancet 381 (9868) (2013) 774–775.
[35] M.V. Maddali, M. Churpek, T. Pham, et al., Validation and utility of ARDS subphenotypes identified by machine-learning models using clinical data: an observational, multicohort, retrospective analysis, Lancet Respir. Med. 10 (4) (2022) 367–377.
[36] M. Cecconi, L. Evans, M. Levy, et al., Sepsis and septic shock, Lancet 392 (10141) (2018) 75–87.
[37] D. Mokrá, Acute lung injury - from pathophysiology to treatment, Physiol. Res. 69 (Suppl 3) (2020) S353–s366.
[38] R.P. Dellinger, J.M. Carlet, H. Masur, et al., Surviving Sepsis Campaign guidelines for management of severe sepsis and septic shock, Crit. Care Med. 32 (3) (2004) 858–873.
[39] R.S. Ferrari, C.F. Andrade, Oxidative stress and lung ischemia-reperfusion injury, Oxid. Med. Cell. Longev. 2015 (2015), 590987.
[40] M. Mittal, M.R. Siddiqui, K. Tran, et al., Reactive oxygen species in inflammation and tissue injury, Antioxidants Redox Signal. 20 (7) (2014) 1126–1167.
[41] Y. Cai, J. Li, C. Jia, et al., Therapeutic applications of adipose cell-free derivatives: a review, Stem Cell Res. Ther. 11 (1) (2020) 312.
[42] C. Li, S. Wei, Q. Xu, et al., Application of ADSCs and their exosomes in scar prevention, Stem Cell Rev Rep 18 (3) (2022) 952–967.
[43] R. Kalluri, V.S. LeBleu, The biology, function, and biomedical applications of exosomes, Science 367 (6478) (2020).
[44] G. Zheng, R. Huang, G. Qiu, et al., Mesenchymal stromal cell-derived extracellular vesicles: regenerative and immunomodulatory effects and potential applications in sepsis, Cell Tissue Res. 374 (1) (2018) 1–15.
[45] M.A. Matthay, S. Pati, J.W. Lee, Concise review: mesenchymal stem (stromal) cells: biology and preclinical evidence for therapeutic potential for organ dysfunction following trauma or sepsis, Stem Cell. 35 (2) (2017) 316–324.
[46] H.F. Yan, T. Zou, Q.Z. Tuo, et al., Ferroptosis: mechanisms and links with diseases, Signal Transduct. Targeted Ther. 6 (1) (2021) 49.
[47] C. Liang, X. Zhang, M. Yang, et al., Recent progress in ferroptosis inducers for cancer therapy, Adv. Mater. 31 (51) (2019), e1904197.
[48] X. Chen, R. Kang, G. Kroemer, et al., Ferroptosis in infection, inflammation, and immunity, J. Exp. Med. 218 (6) (2021).
[49] J. Zheng, M. Conrad, The metabolic underpinnings of ferroptosis, Cell Metabol. 32 (6) (2020) 920–937.
[50] J.S. Bednash, V.E. Kagan, J.A. Englert, et al., Syrian hamsters as a model of lung injury with SARS-CoV-2 infection: pathologic, physiologic, and detailed molecular profiling, Transl. Res. 240 (2022) 1–16.
[51] S. Li, M. Shi, Y. Wang, et al., Keap1-Nrf2 pathway up-regulation via hydrogen sulfide mitigates polystyrene microplastics induced-hepatotoxic effects, J. Hazard Mater. 402 (2021), 123933.
[52] B. Chen, Y. Sun, J. Zhang, et al., Human embryonic stem cell-derived exosomes promote pressure ulcer healing in aged mice by rejuvenating senescent endothelial cells, Stem Cell Res. Ther. 10 (1) (2019) 142.
[53] N. Lerner, I. Chen, S. Schreiber-Avissar, et al., Extracellular vesicles mediate anti-oxidative response-in vitro study in the ocular drainage system, Int. J. Mol. Sci. 21 (17) (2020).
[54] J.H. Yeo, M.M. Chong, Many routes to a micro RNA, IUBMB Life 63 (11) (2011) 972–978.
[55] R. Garcia-Martin, G. Wang, B.B. Brandão, et al., MicroRNA sequence codes for small extracellular vesicle release and cellular retention, Nature 601 (7893) (2022) 446–451.
[56] C. Ma, X. Qi, Y.F. Wei, et al., Amelioration of ligamentum flavum hypertrophy using umbilical cord mesenchymal stromal cell-derived extracellular vesicles, Bioact. Mater. 19 (2023) 139–154.
[57] J.C. Jann, M. Mossner, V. Riabov, et al., Bone marrow derived stromal cells from myelodysplastic syndromes are altered but not clonally mutated in vivo, Nat. Commun. 12 (1) (2021) 6170.
[58] J. Chen, J. Chen, Y. Cheng, et al., Mesenchymal stem cell-derived exosomes protect beta cells against hypoxia-induced apoptosis via miR-21 by alleviating ER stress and inhibiting p38 MAPK phosphorylation, Stem Cell Res. Ther. 11 (1) (2020) 97.
[59] D. Rittirsch, M.S. Huber-Lang, M.A. Flierl, et al., Immunodesign of experimental sepsis by cecal ligation and puncture, Nat. Protoc. 4 (1) (2009) 31–36.